Chaotic Escape of Photons from a Fish-Shaped Reflecting Cavity

A thesis submitted in partial fulfillment of the requirement
for the degree of Bachelor of Science with Honors in
Physics from the College of William and Mary in Virginia,

by

Paul C. Hansen

Accepted for

_____

_____

Advisor: Prof. John B. Delos

_____

Prof. Henry Krakauer

_____

Prof. Nahum Zobin

Williamsburg, Virginia

May 2004

Contents

Acknowledgments

Many thanks to...

Kevin Mitchell for helpful mathematical discussions during this project

Hurricane Isabel for sparing my computer and giving me a nice break in the mountains

Prof. Delos, my thoroughly excellent advisor, for being available for consultation whenever I walked into his office!

S.D.G.

List of Figures

Abstract

We consider the escape of a microwave photon or a particle bouncing ballistically from an open, fish-shaped reflective cavity. Trajectories within the cavity may be chaotic, regular or periodic, so not all initial conditions lead to escape. Rather, if we fix the initial position of the photon and record escape time as a function of the initial direction, the resulting escape-time diagram shows "epistrophic fractal" structure—repeated structure within structure at all levels of resolution, with new features introduced into the fractal at longer time scales. At an external detector an observer would note a characteristic pulse train of escaping particles. We approach the problem through simulation using Matlab, but the setup is simple and lends itself to verification in the laboratory.

Chapter 1

Introduction

1.1 Background

We study a system involving "chaotic escape"—the system is open, so trajectories may enter and leave, but the amount of time spent within the system is a highly-sensitive function of initial conditions. Nearby trajectories diverge exponentially over time, so it is effectively impossible to predict behavior of specific trajectories over long time scales. However, governing principles exist which qualitatively *and* quantitatively describe the behavior of sets of trajectories. Some of these principles have been known for years: for example, scientists have known for several decades that chaotic systems often exhibit fractal structure in various ways (a fractal is a figure with self-similar features at all levels of resolution). Well known fractals show regular self-similarity (*e.g.* the Cantor set), asymptotic self-similarity (*e.g.* sequences of period-doubling bifurcations) or statistical self-similarity (*e.g.* coastlines and clouds) [3]. But under certain circumstances, a chaotic system may exhibit a fourth type of fractal structure

called epistrophic self-similarity. Kevin Mitchell of William and Mary has recently developed a quantitative interpretive structure for these epistrophic fractals, known as homotopic lobe dynamics, which explains much but not all of the observed structure [4]. The present system was chosen to meet the criteria for epistrophic self-similarity (to be listed later) and provides a test case for application of Mitchells mathematics.

1.2 Related Work

Tiyapan and Jaffé [6] analyzed a chaotic scattering system in the early 1990s. In the scattering of He from I_2, depending on its intial position and momentum the helium atom may be temporarily trapped in a potential well around the iodine. The initial angle-final action plot is smooth for most initial angles but assumes a very complicated structure for a small set of angles. Within this chaotic region, contiguous segments of initial angles map smoothly to the final action, but in between these segments the final action varies wildly (Miller uses the term "chattering trajectories"). The smooth segments of initial conditions, called icicles for their pointed appearance, form patterns that repeat at all scales. Tiyapan and Jaffé examined these patterns at seven levels of resolution and gave evidence of asymptotic self-similarity between the icicles each level. Groups of icicles form a convergent infinite series which Mitchell *et al.* call an epistrophe.

Recently, analogous phenomena in the escape of high-Rydberg electrons from hydrogen atoms in parallel electric and magnetic fields have been found [5]. This system is one of the simplest possible that allows chaos. The motion of a highly-excited electron near a proton is well understood from classical mechanics, and is not chaotic: the

proton creates a potential well and the electron moves in an elliptical, parabolic or hyperbolic trajectory depending on its energy. Under application of a constant electric field, the electrons orbits stretch, and for a strong enough field even the tightly bound orbits will be ripped from the proton. In this case, the equations of motion are separable, and the trajectories remain regular. The application of a magnetic field couples the degrees of freedom: the magnetic force $F = qV \times B$ accelerates the electron perpendicularly and brings on chaotic dynamics. Under parallel electric and magnetic fields, the spherical inverse-square potential well is deformed into a teardrop shape, roughly centered at the proton but pinching into a saddle point downstream in the electric field. Electrons may only escape by crossing this saddle point. Unlike the zero-field case, energy alone does not determine whether an electron is bound or unbound—rather, the time taken for an excited electron to escape over the saddle region depends sensitively on the combination of initial position and velocity. Two electrons of equal energy, starting on only slightly different trajectories, may escape at very different times; one may escape early while the other remains trapped in wild orbits around the proton forever.

Mitchell simulated sets of trajectories of equal energy and studied the relationship between initial angle and time to escape. Trajectories which head straight for the saddle point may escape very quickly, but if they aim too far to the side they will oscillate laterally and fail to cross the saddle, eventually falling back into the well and winding around the proton again. The set of intial angles leading to quick escape form an "escape segment in Mitchell's plot. Sets of nearby initial conditions that orbit the proton once before escape form secondary escape segments; in fact, the segments e_n of the initial angular distribution which escape in n transverse oscillations form an infinite series, each segment growing exponentially narrower. We can see structure-

within-structure in this escape-time plot, and on closer examination we would find infinite sequences which display asymptotic self-similarity.

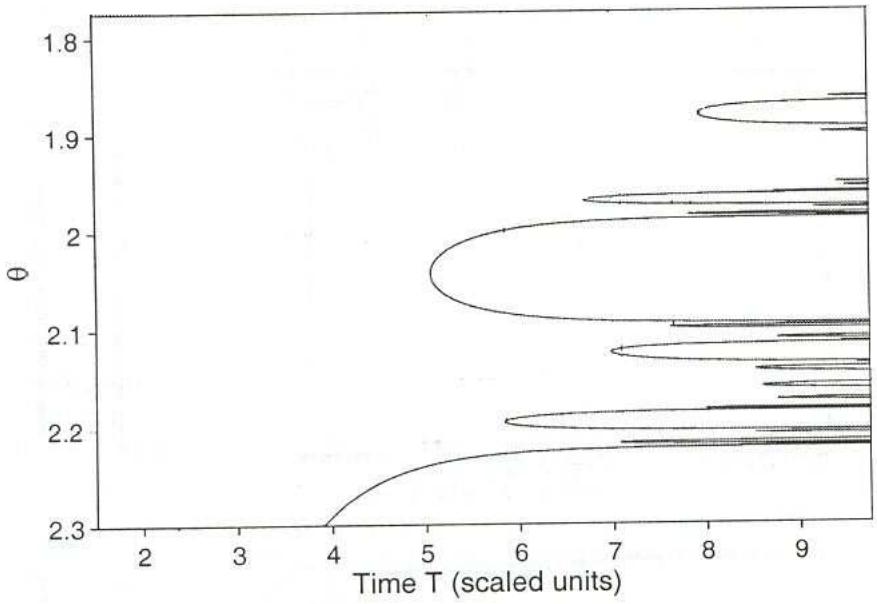

Figure 1.1: **Time To Escape in Ionization of Hydrogen**

These escape segments are only the first of many layers of order in the escape-time plot. However at longer times there appear "unexpected" escape segments which Mitchell *et al.* call "strophes." These strophes break the pattern of earlier escape segments. At very long time scales, the strophes come to dominate the fractal. Such epistrophic fractals, developing new order at high levels of resolution, appear in many chaotic systems. We see hints of this behavior in Figure 1.1, and we will give examples from our system later.

Mitchell found a mathematical way to predict epistrophes by examining the *phase plane*—the plot of a single coordinate and its related momentum. The resulting "homotopic lobe dynamics" is applicable to many chaotic systems, provided that they satisfy certain criteria (given in [3], [4]). The short-time behavior of the hydrogen

system is fully described by Mitchells method, but the unexpected strophic escape segments are not yet fully accounted for.

Over the summer of 2003, REU student Melissa Commisso began work on the present project, simulating the escape of photons from a fish-shaped reflective cavity (Figure 1.2) [1]. This system was conceived as a more lab-friendly alternative to the hydrogen ionization experiments—it features similar dynamics and produces analogous escape-time fractals, but the physical experiments may be performed using microwaves in two dimensions on a lab table. Commisso used Maple to model the cavity and trajectories, and produced escape-time plots showing escape segments and structure within structure. Unfortunately Maple proved to be an inadequate tool for such programmatic tasks and hindered progress substantially.

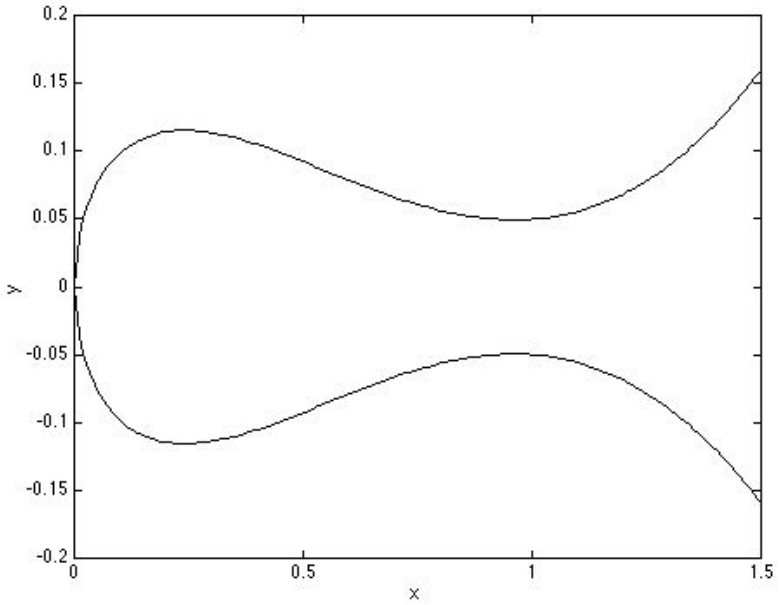

Figure 1.2: **Fish Cavity**

Beginning in Fall 2003, we rewrote the simulator using Matlab and carried out nu-

merical experiments similar to Mitchell's hydrogen simulations. In Chapter 2 of this paper we give a physical overview of the system, including the choice of the cavity shape and possible resulting trajectories. Then we give a primer on dynamics in the phase plane and a qualitative overview of the results, particularly the epistrophic fractal structure in the escape-time plot and resulting characteristics of the outgoing pulse train. Chapter 3 is solely devoted to homotopic lobe dynamics, and Chapter 4 applies those techniques to our phase plane to explain our escape-time plots and predict features at all levels of resolution. The appendix presents technical details of our implementation.

Chapter 2

The System

2.1 The Cavity

The shape of a reflecting cavity determines the types of trajectories that may propagate inside it. Practically speaking, a cavity that superficially resembles the hydrogen saddle potential supports similar chaotic dynamics (Figure 2.1). In the hydrogen system, an electron may be trapped in a stable region in which it orbits the proton for all time. The reflecting cavity must provide a similar stable region in which photons may bounce back and forth without escape. Electrons may only escape the hydrogen system by passing the saddle point, and if they fail to cross they will turn slowly and return for another orbit in the well. Likewise, the reflecting cavity must have a bottleneck that allows escape for certain trajectories but turns back trajectories with too much transverse motion. Electrons that cross the saddle point in the hydrogen system never return; the outside of the reflecting cavity must flare to prevent escaped photons from returning before reaching an external detector. Lastly, the cavity must

be relatively smooth to minimize discontinuities in the dynamics—nearby trajectories can diverge over a sequence of bounces but they should not be abruptly split apart by cusps or corners. Our system does feature one discontinuity associated with the curvature in the narrow region, but in the present case this does not complicate the dynamics.

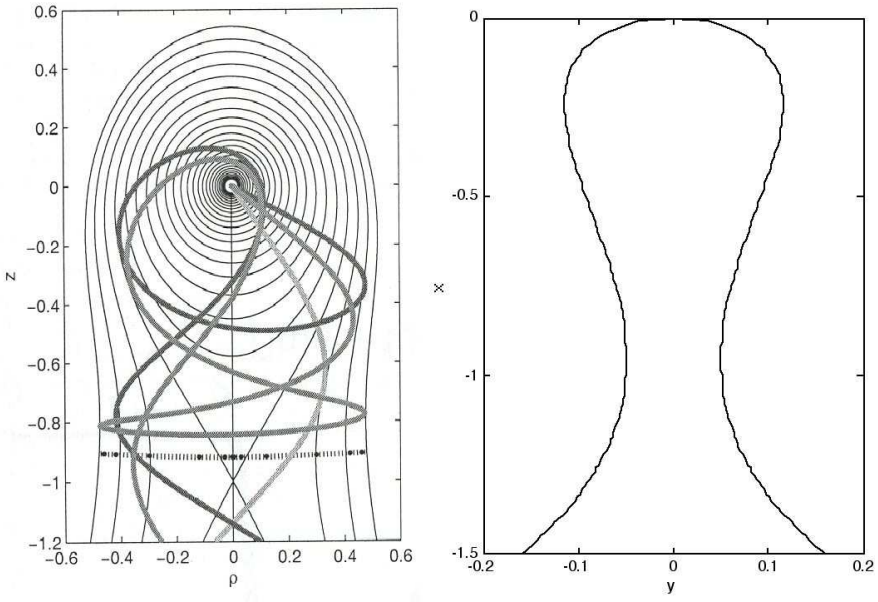

Figure 2.1: **Hydrogen Potential and Fish Cavity,** with e^- trajectories

Let us think about stability and instability of orbits. Consider a two-dimensional circular cavity. A photon released on a diameter of this circle will remain on that diameter forever, bouncing back and forth (Figure 2.2). However under slight perturbations of the initial angle, the photon will precess around the entire circle at a constant rate. This is known as neutral stability—nearby trajectories move apart linearly in time. However, if two pieces were cut from the circle and the remaining arcs were brought together, trajectories between the two walls would be stably confined forever. On the other hand, were the two arcs separated by more than the original

diameter, trajectories would be unstable and escape.

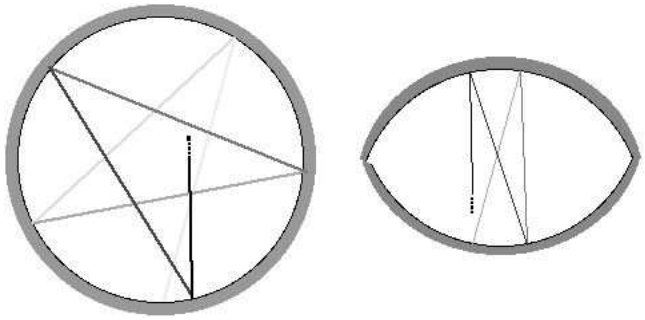

Figure 2.2: **Neutrally Stable and Stable Orbits**

Consider also a pair of facing convex surfaces (Figure 2.3). Classically a photon could bounce ballistically between the extrema of these surfaces forever. However, this orbit is unstable—if perturbed, it will exponentially diverge from the transverse orbit.

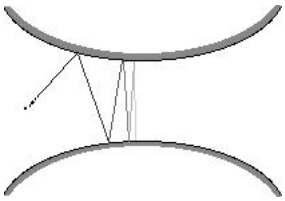

Figure 2.3: **Unstable Orbits**

To combine these unstable and stable regions into one surface, we compose several parabolic sections (Figure 2.1). The first, forming the nose of the fish, faces outward along the x-axis. Further along the positive x-axis we create a hyperbolic-like bottleneck by pairing two parabolas oriented outwards in the y-direction (Figure 2.4). We multiply the parabolas to combine them into one surface. The shape can be further fine-tuned by adjustment of three parameters: A, the steepness of the bottleneck; w, the width of the bottleneck region; and L, the position of the bottleneck on the x-axis. Practically speaking, A is the means to adjust the height of the cavity, and modifying A is sufficient to alter the systems dynamics. Early on we set $L = 1$ and

$w = 0.2$ (in arbitrary units); we have not changed them since.

$$y = f(x) = \pm\sqrt{x}\left(\frac{w}{2} + A(x - L)^2\right) \tag{2.1}$$

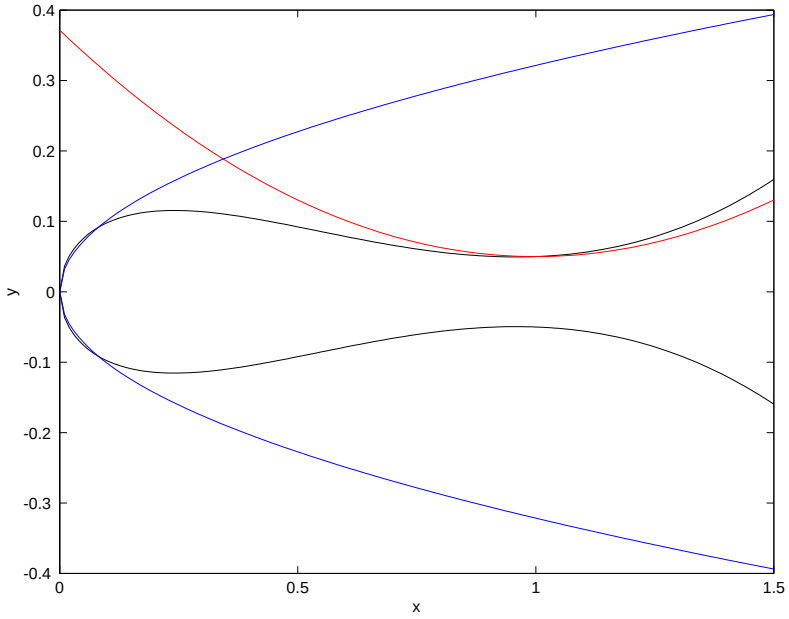

Figure 2.4: **The Fish Cavity** with parabolic factors

We position a simulated "detector" at $x = 1.5$, well outside the bottleneck. In the simulation it is sufficent to say that this is where trajectories end. In the lab, this could be an absorbing boundary, or one might put a small microwave detector at various points along this boundary.

2.2 Types of Trajectories

We release an ensemble of trajectories from a point on the wall of the cavity, representing the wavefront of a microwave burst. We graph such a set of trajectories

between the initial point and the first bounce (Figure 2.5). Photons bounce off the walls ballistically without attenuation. We let $c = 1$, so distance traveled is the same as time elapsed.

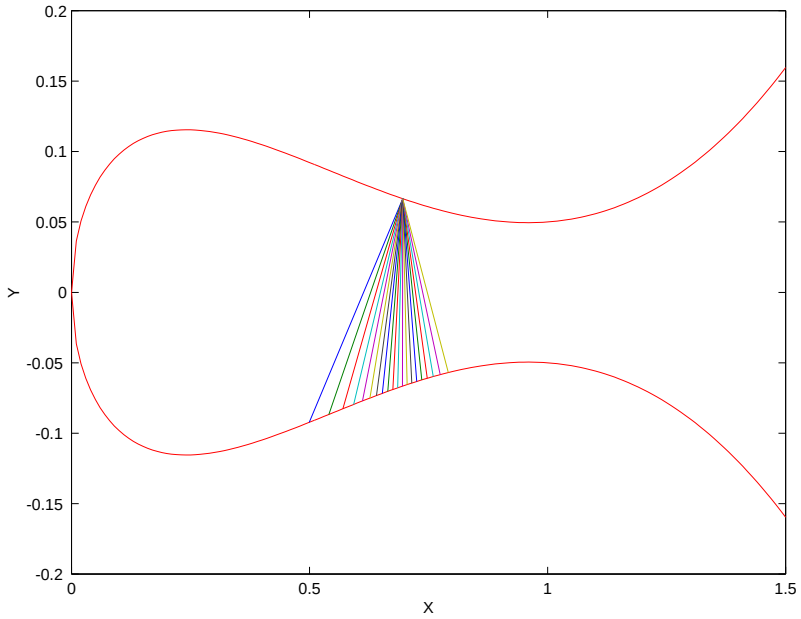

Figure 2.5: **Initial Ensemble of Trajectories**

Trajectories may be periodic (stable or unstable), regular or chaotic depending on their initial conditions. In this system, whether and when a photon eventually escapes depends on its initial position and direction of motion. The simplest stable trajectory is the straight-across bounce in the middle of the cavity. Every two bounces takes the photon back to the same place, hence we call this a period-2 stable orbit. Quasi-periodic orbits oscillate or precess about the period-2 orbit in the middle. Other periodic orbits are also possible, with periods from three to infinitely many bounces.

Regular scattering trajectories can be harder to pick out visually because they are not restricted to a narrow band of the cavity. They escape quickly after being released, and once they head in the direction of the bottleneck they will not return to the

cavity. The most recognizable regular trajectories are the whispering gallery modes which stay close to the wall of the convex region before escaping. None of the regular trajectories are particularly interesting and we usually omit as many of them as possible from our initial ensembles.

The chaotic trajectories occupy the region between regular scattering and stable trajectories. Photons that approach the bottleneck several times before finally escaping follow chaotic trajectories. A chaotic orbit may remain in the cavity forever without once repeating its position and velocity. As with the hydrogen system, the escape-time plot for a set of chaotic trajectories forms an epistrophic fractal.

Examples of stable, unstable and regular scattering trajectories are shown in Figure 2.6.

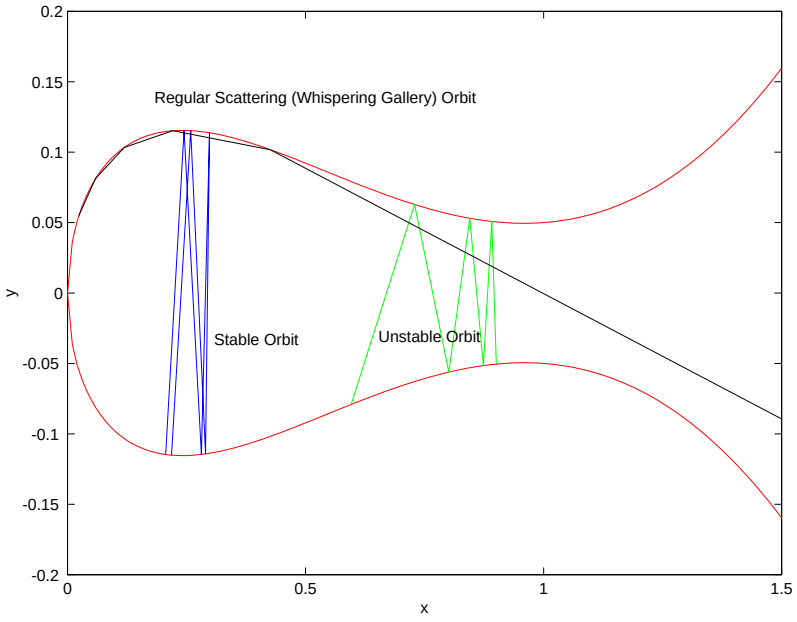

Figure 2.6: **Trajectories In The Fish Cavity**

Let us consider continuity and uniqueness of trajectories. The methods of homotopic

lobe dynamics assume that the system can be modeled by an continuous area- and orientation- preserving saddle-center map. Among other things, this means that continuously changing a trajectory's initial conditions will continuously change all its future positions and velocities. If a photon begins at (x_0, v_0) and next bounces to (x_1, v_1), a smooth change in (x_0, v_0) should never result in a discontinuous jump in (x_1, v_1). There is in fact a possible discontinuity, due to concavity in the bottleneck region, where the transition between trajectories from inside that brush the bottleneck and escape directly to the detector is abrupt. Fortunately this discontinuity does not affect dynamics inside the cavity.

Uniqueness of trajectories means that if two trajectories are ever at the same point with the same velocity, they will continue to be the same for all time (past and future). The combination of uniqueness and continuity permits powerful topological arguments about ordering of trajectories in the future.

2.3 The Phase Plane

All the defining characteristics of the cavity and trajectories within it may be understood in the phase plane. For a system with two degrees of freedom, it may be sufficient to focus on just one generalized coordinate and its associated momentum. We found that the best coordinate and momentum in our system are the distance l along the wall where each bounce occurs and the momentum p_l parallel to the wall at that bounce. For every bounce we plot l and p_l; a single trajectory will form a series of dots on this surface of section. By this method we uncover essential features of the system that are difficult to see by watching trajectories propagate in the cavity, such

as stable and unstable regions of the phase plane, stable fixed points and periodic orbits, stable and unstable manifolds of unstable fixed points, and regions of chaos. These terms will be introduced by examples from the fish-cavity system. In fact the simple ideas of continuity and uniqueness of trajectories in the cavity are corollaries of deeper ideas in the phase plane, often related to ideas from ordinary differential equations.

2.3.1 The Arc Length Surface Of Section

Assign to each point on the cavity wall a coordinate l equal to the clockwise distance from the origin (the nose of the fish) (Figure 2.7). When a photon strikes the wall its associated momentum p_l is the component of its velocity vector parallel to the wall (recall $p = v = c = 1$ in simulation units). A regular whispering gallery trajectory maintains a large (nearly 1.0 or -1.0) p_l along the interior of the cavity (Figure 2.8).

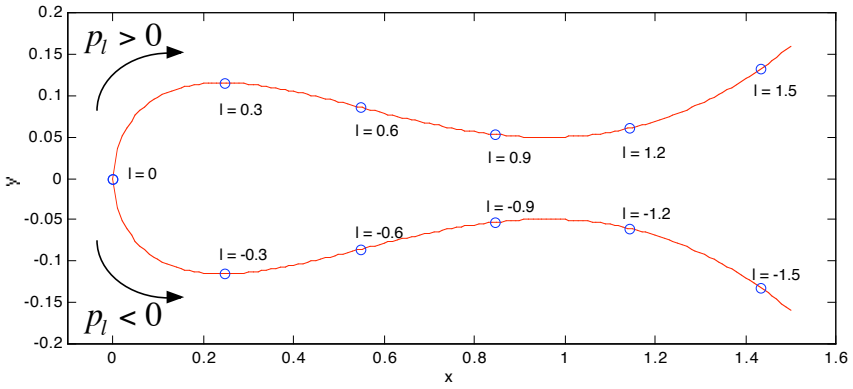

Figure 2.7: **Arc Length Coordinates**

The trajectory in Figure 2.6 is confined to the top wall of the cavity where $l > 0$. As a result its trace in the phase plane remains on the right of the origin. However most trajectories leave traces alternating between $l < 0$ and $l > 0$. Consider an

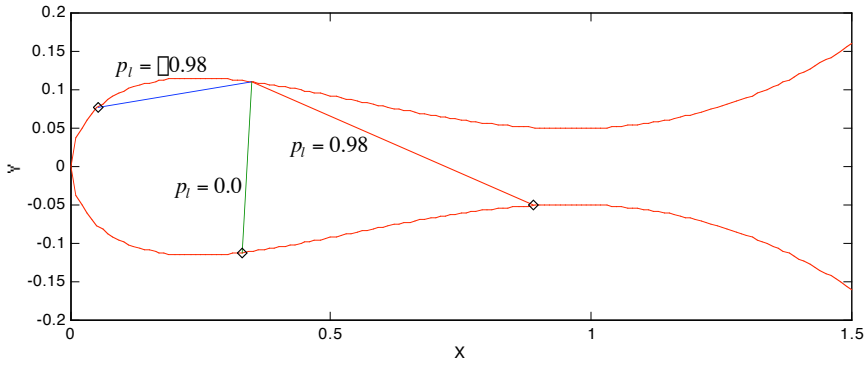

Figure 2.8: **Arc Length Momenta**

orbit released in the bottleneck region, drifting left into the cavity (Figure 2.9). Its cartesian momentum p_x is negative at each bounce, but p_l is positive for bounces at the bottom of the cavity ($l < 0$) and negative for bounces at the top ($l > 0$). Points on the surface of section thus alternate between the second and fourth quadrants. Likewise the primary stable and unstable period-2 orbits alternate between the left and right sides of the surface of section, with $p_l = 0$.

Let us introduce a simplification to take advantage of the fish curves reflection symmetry in y. In the original surface of section, the orbits in Figure 2.9 leave symmetric or quasi-symmetric paths; the natural odd-symmetry suggests that all points $(l < 0, pl)$ be reflected through the origin. Suppose we place a reflecting boundary on the x-axis ($y = 0$). Then any orbit which would have gone from the top of the fish ($l_0 > 0$) to the bottom of the fish ($l_1 < 0$) is actually reflected to the point $(-l_1 > 0, -p_{l1})$. Therefore when we run the map $(l_0, p_{l0}) \rightarrow (l_1, p_{l1})$, we may add a condition: if $l_1 < 0$, then replace (l_1, p_{l_1}) by $(-l_1, -p_{l1})$. In the new surface of section a stable period-2 orbit looks like a single point, and any other orbit traces a single succession of points in the phase plane (Figure 2.10).

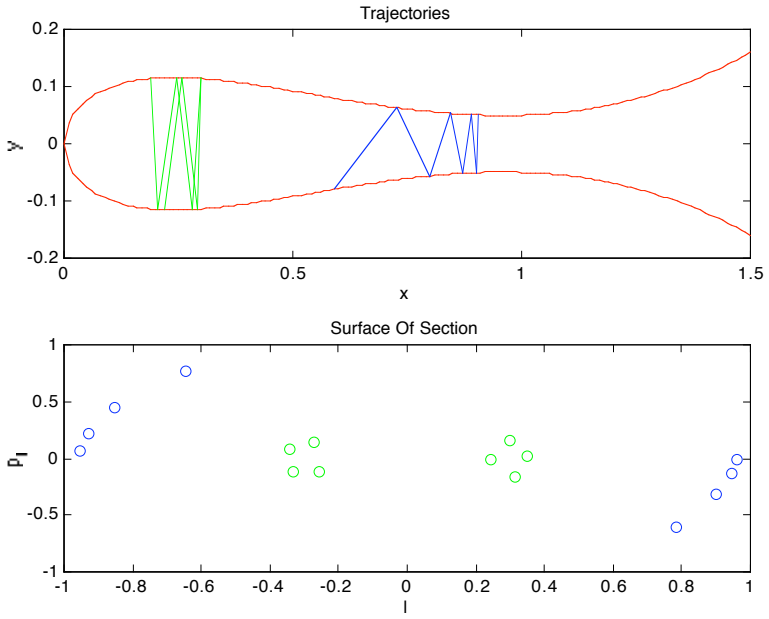

Figure 2.9: **Stable and Unstable Orbits in the Phase Plane**

This reflected surface of section retains all the information of the old one. True, there is no longer a distinction between a bounce on the bottom of the curve and a bounce on the top. However, it has already been shown that these situations are effectively identical: the mapping between reflecting pairs of trajectories and paths in the surface of section is still one-to-one. The simplified mapping is now easily lined up with the diagram of the fish cavity (as in Figure 2.11). The phase plane provides the best means to analyze nonlinear systems and retains all the information from the cavity diagrams, hence from now on we shall study events in phase plane rather than events in the cavity.

The orbits in the cavity induce a map M on the surface of section. The map converts photon position and velocity at one bounce to new position and velocity at the next bounce in the cavity. Five iterates of the map trace a five-bounce trajectory from one initial condition. M is a map from the phase plane to itself, so we may plot the evo-

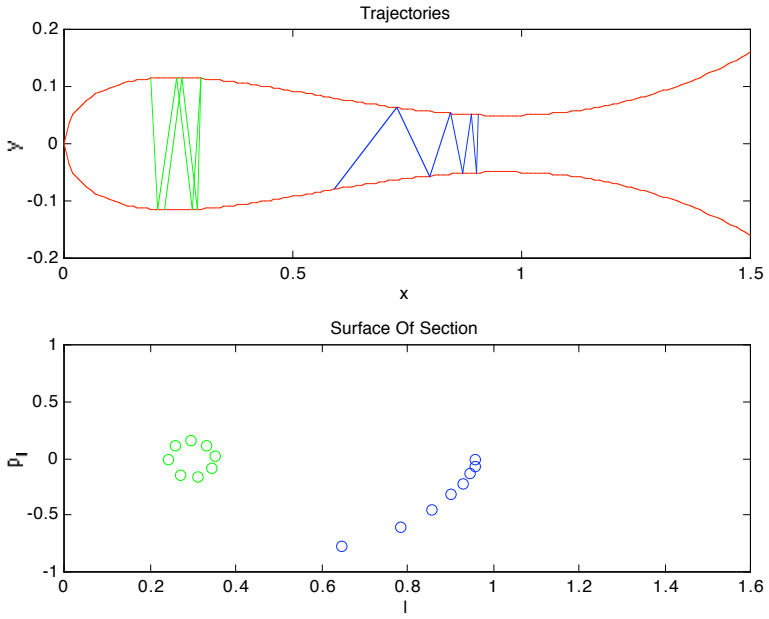

Figure 2.10: **Reflected Surface of Section**

lution of orbits under repeated applications of M. The most important features of M depend on the location and character of fixed points, points that map to themselves.

Any period-2 orbit in the cavity looks like a fixed point in the surface of section. Two have special importance: the stable period-2 orbit in the center of the cavity and the unstable period-2 orbit in the bottleneck region. A stable fixed point is surrounded by concentric rings formed by perturbations of that orbit. These rings give the alternative name "O-points" to stable fixed points (note that higher-period stable orbits feature multiple O-points). In a system such as a simple harmonic oscillator, these concentric rings belong to trajectories of specific constant energies; in our nonlinear system the concentric rings belong to different initial conditions.

We designate the unstable fixed point in the bottleneck as the *principal unstable fixed point*. Trajectories near this point either turn back into the cavity or bounce out to

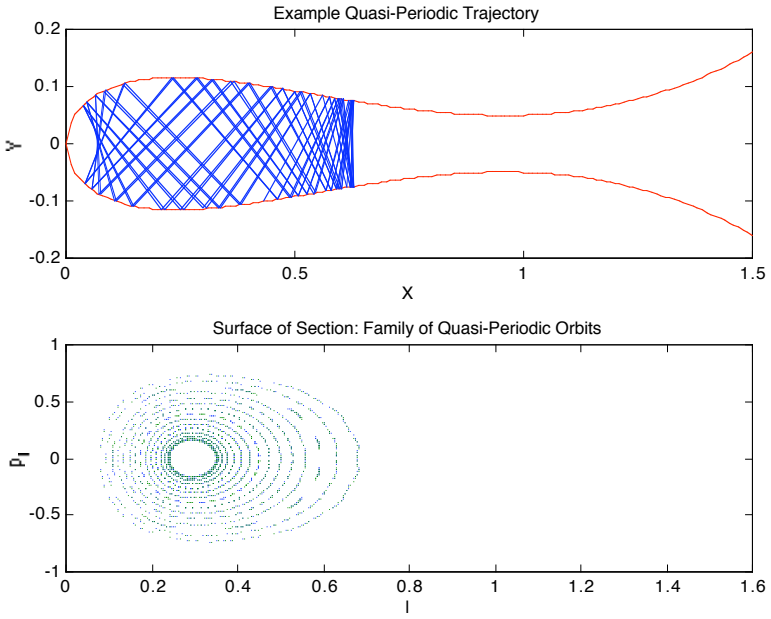

Figure 2.11: **Quasi-Periodic Orbits**

the detector, so there are no concentric rings as around a stable fixed point. Rather, orbits near an unstable fixed point accelerate outwards in opposite directions along a line in the surface of section. This line is called the *unstable manifold* (alternatively, *out-set*) of the unstable fixed point. Similarly, the *stable manifold* (alternatively, *in-set*) is the set of all trajectories that map into the unstable fixed point. Due to symmetry in the fish curve, the stable manifold is the reflection of the unstable manifold with $p_l \to -p_l$. The manifolds meet transversely at the unstable fixed point, marking it as an X-point. We graph portions of the two manifolds in Figure 2.12.

Every point on the stable or unstable manifold continues to map onto that manifold for all time. This includes the homoclinic points marking intersections between the stable and unstable manifolds. One may easily prove that the existence of one homoclinic point implies the existence of an infinity of homoclinic points converging on the X-point along both manifolds. Hence the manifolds cross and re-cross infinitely many

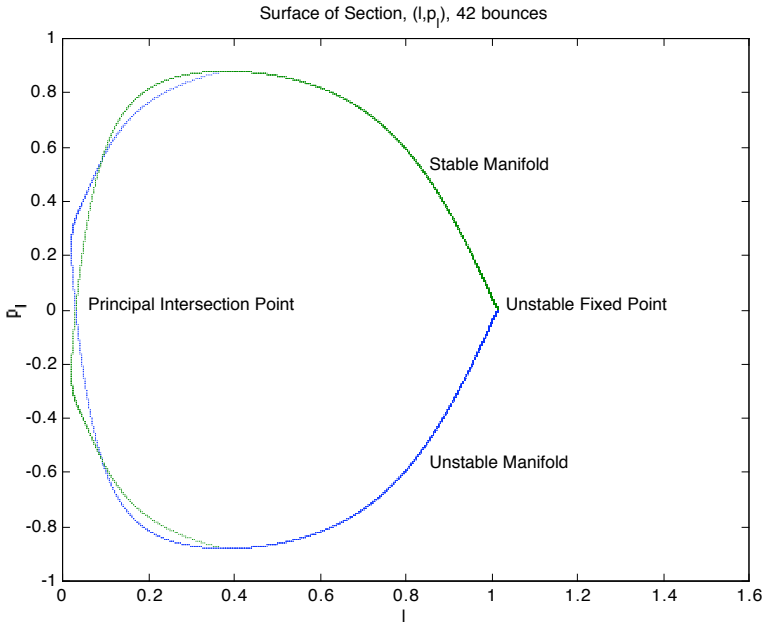

Figure 2.12: **Stable and Unstable Manifolds**

times in a wildly complicated homoclinic tangle (Figure 2.13). Going forward in time, each homoclinic point maps towards the X-point along the stable manifold; going backward in time, the pre-images of each homoclinic point converge towards the X-point along the unstable manifold.

How can an infinity of homoclinic points fit onto the finite segments of both manifolds from the unstable fixed point to the principal homoclinic point, if chaotic trajectories diverge exponentially? We make a comparison to a simple system of differential equations: linearize the map M, connecting it to an iterative solution to a pair of linear ordinary differential equations. The two eigenvectors lie parallel to the stable and unstable manifolds; the eigenvalues are the rates of exponential divergence outward along those directions. Hence the unstable manifold must attract nearby trajectories, and the stable manifold must repel nearby trajectories (under time-reversal the opposite holds).

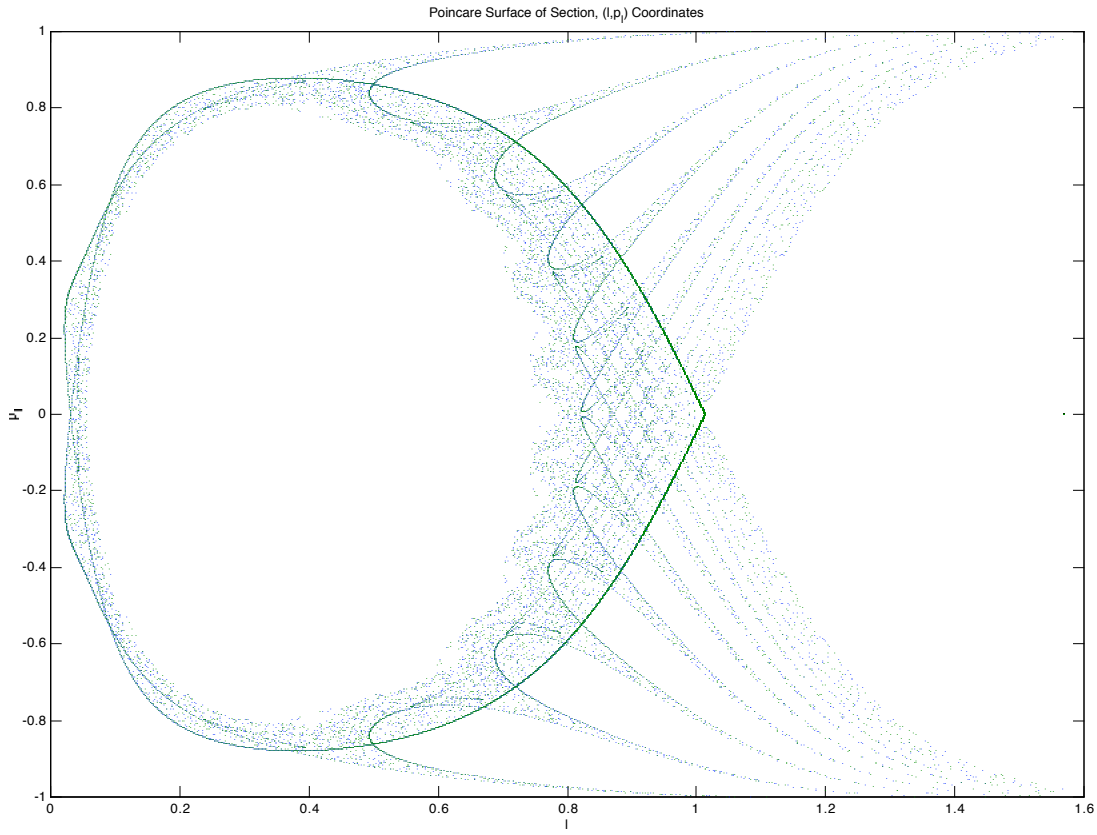

Figure 2.13: **Homoclinic Tangle**

Now consider a set of initial conditions surrounding the X-point. As they map forward they converge upon the unstable manifold and accelerate exponentially along it. At each mapping, the set of trajectories distorts along the unstable manifold, lengthening and narrowing proportionally to the eigenvalues of the map at the X-point. As will be discussed shortly, the map preserves area, and it follows that the two eigenvalues are reciprocals of each other. The larger of the two eigenvalues, the *Liapunov exponent* of the principal unstable fixed point, determines the rates of convergence and divergence of trajectories in the phase plane.

2.3.2 Implications Of Continuity And Uniqueness Of Trajectories

By the one-to-one mapping of cavity trajectories to phase plane trajectories, continuity and uniqueness of trajectories now becomes continuity of the map and uniqueness of trajectories on the surface of section. Uniqueness of trajectories is already obvious—the simulator map M cannot assign two images to one point in the phase plane. Actually we can safely extend uniqueness to entire stable and unstable manifolds made of an infinity of trajectories: neither the stable nor the unstable manifold can cross itself. Continuity of the orbits, together with certain properties of Hamiltonian dynamical systems, implies that M is a continuous area- and orientation-preserving map on the phase plane (except in escape regions).

- Continuous: M preserves properties of sets. Connected sets remain connected; points map to points, curves map to curves, connected regions map to connected regions.
- Area-preserving: the measure of a connected set will remain constant under M. Shapes can deform but areas will be preserved. This is proven in the linearized area near an unstable fixed point by equality of eigenvalues, but is also true in the entire phase plane. There is one exception to the rule: after escaping from the cavity the point maps to infinity. Then area preservation is meaningless.
- Orientation-preserving: a right-handed intersection of two directed curves maps to another right-handed intersection of two directed curves.

We may apply these properties to entire lobes bounded by the stable and unstable manifolds (Figure 2.14). Because the manifolds cross at alternate right- and left-

handed homoclinic points, orientation preservation implies that each homoclinic point maps to its second neighbor: there are two infinite interlaced sequences of homoclinic points. These alternating points bound two sets of lobes that map into themselves; by area preservation the lobes must have equal areas as long as none of the points maps to infinity.

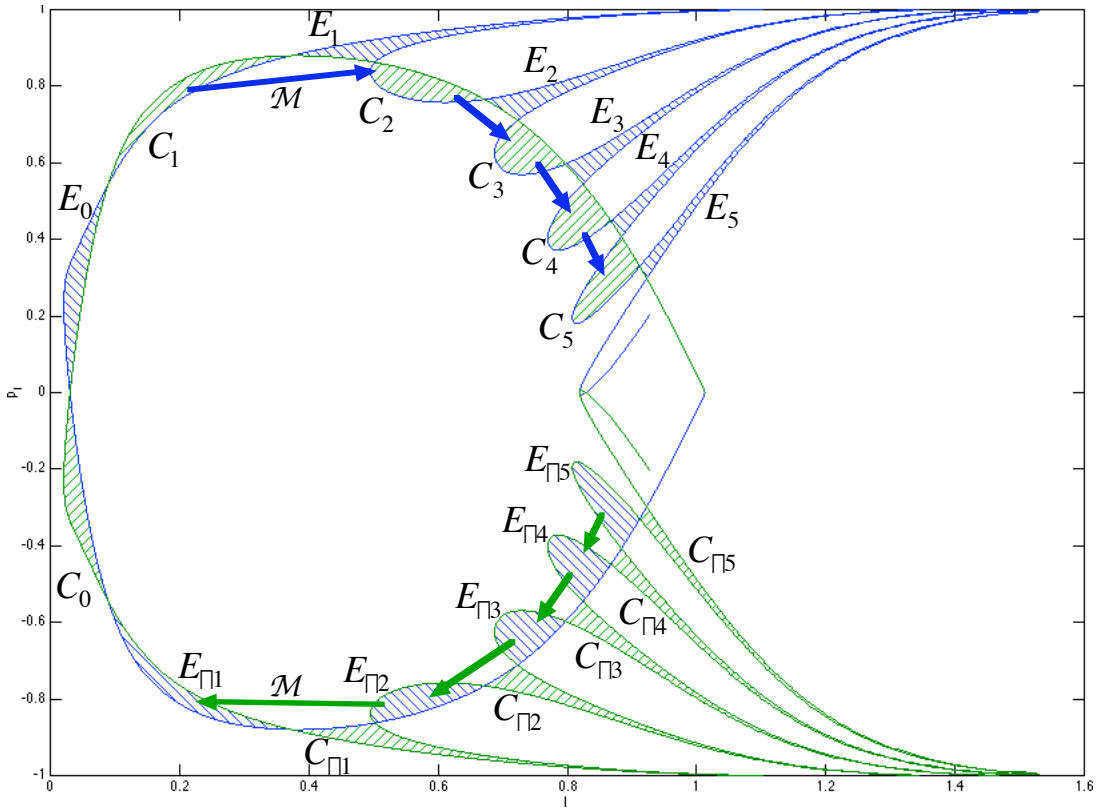

Figure 2.14: **Lobes in the Phase Plane**

2.3.3 Homoclinic Tangles

Henri Poincaré discovered the properties of homoclinic tangles over one-hundred years ago; Chapter 3 introduces the newer homotopic lobe dynamics for describing these

tangles. In the meantime several more features the map deserve attention: island chains, discontinuities in the escape region, and the region of regular trajectories.

A relatively complete phase portrait of the system (Figure 2.15 includes a sequence of independent O-points bounds the stable region. The center of each island belongs to the same trajectory, in this case period-10. Orbits slightly displaced from this period-10 stable orbit map out sets of concentric rings around the O-points: the first ring around each of the ten O-points belongs to one trajectory. An X-point lies between each pair of adjacent O-points in the island chain, with its own stable and unstable manifolds. When the manifolds of separate X-points cross, they form small *heteroclinic tangles* of infinite complexity, which sometimes interact with the tangle of the principal unstable fixed point. Island chains often are present in the boundary region between stability and chaos, and they cause increased complexity of escape-time plots.

As already mentioned, if a trajectory escapes from the cavity, it may go to infinity with no further bounces. In this case the area-preservation in the map becomes meaningless. Indeed the escaping lobes do not share the same area. As will be discussed in depth later, these lobes are regions from which trajectories may escape to the detector in one bounce. Fortunately any lobe which does not lose trajectories will map to a lobe of the same area.

The entire region outside the stable and unstable manifolds is the domain of regular scattering trajectories. These trajectories tend to escape in a short time. If a simulation includes a lot of regular trajectories they will dominate the early part of the escape-time diagram; the behavior featuring fractal structure begins after the regular trajectories have all escaped. Usually the regular initial conditions are omitted from

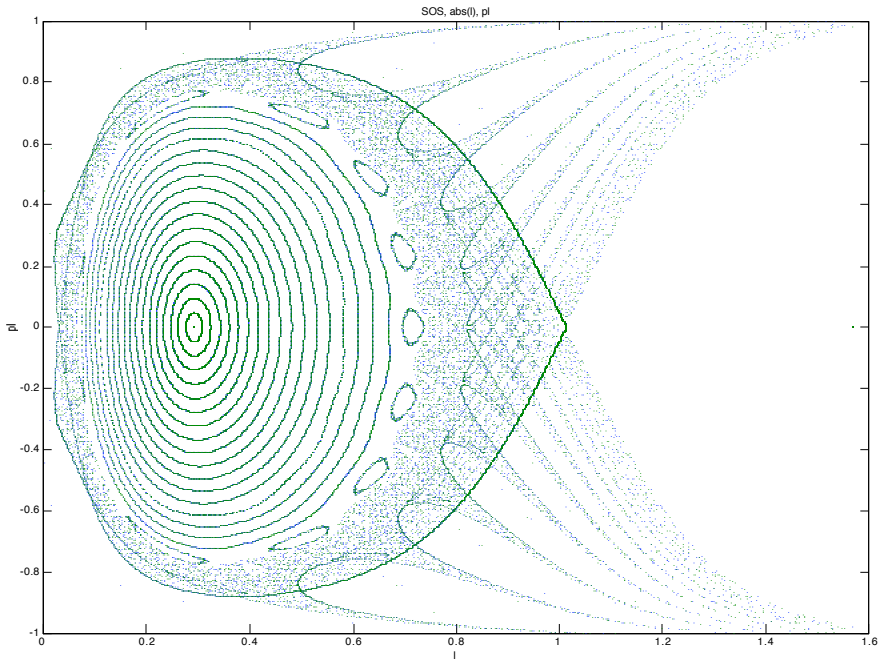

Figure 2.15: **Phase Portrait of the Fish Cavity System**

our runs for this reason.

2.4 Procedure and Description of Results

With the prerequisite information and mathematics in place, we present the basic calculation and results, deferring full analysis to Chapter 4. We show that the system is analogous to the hydrogen system in its essential features: time to escape plotted as a function of initial p_l includes escape segments organized into infinite converging sequences called epistrophes; epistrophes spawn new epistrophes at all levels of resolution; unexpected new escape segments called strophes appear at longer times and spawn epistrophes of their own. The escape segments thus comprise an epistrophic fractal. The geometric rate of shrinking of escape segments notably asymptotes to the

Liapunov exponent of the principal unstable fixed point, suggesting that this fractal structure is intimately linked to the infinite converging sequences of homoclinic points on the stable and unstable manifolds.

2.4.1 Method

Select a vertical line of initial conditions L_0 in the phase plane, between (l_0, p_{l0}) and $(l_0, -p_{l0})$ where $l_0 < l_{unstable}$. This specifies an outgoing wavefront from a single emission point on the cavity wall. Photons propagate in all directions from this point, from nearly parallel to the wall ($p_l = \pm 1.0$) to normal to the wall ($p_l = 0$). Sample the line of initial conditions by choosing N uniformly distributed points in the phase plane from $(l_0, -p_{l0})$ to (l_0, p_{l0}) [1]. As an example, a line of twenty-five initial points is shown below in the phase plane, with its accompanying initial trajectories in the cavity (Figure 2.16). (We plot portions of the stable and unstable manifolds for reference).

Of note: the initial conditions near the middle of L_0 intersect the stable zone and map within the cavity forever as stable orbits. Other initial conditions within the bounds of the two manifolds begin chaotic trajectories which escape in various amounts of time, sensitively dependent on the exact initial velocity. Many initial conditions are outside the stable and unstable manifolds, with $|p_l| \gtrsim 0.6$. These represent regular scattering trajectories, and they escape quickly, *e.g.* around the wall of the cavity in whispering gallery modes.

Let us represent the trajectories in the phase plane one bounce at a time. The line of

[1] Uniformity is convenient but not essential to the results.

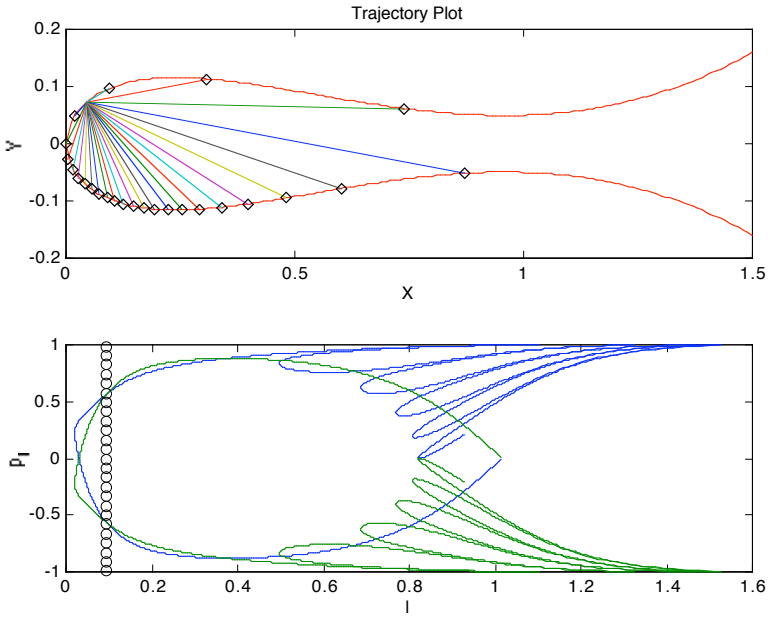

Figure 2.16: **Line of Initial Conditions**

initial conditions maps into a curve, rotated clockwise and sheared in the phase plane (Figure 2.17). We continue this until most of the trajectories escape, then plot each photons time to reach the detector (or distance traveled) as a function of its initial momentum pl0. The result for 1000 photons after forty bounces is shown in Figure 2.18.

2.4.2 Results

The time to escape is jagged, with many singularities. Certain points along the line of initial conditions are local minima of the time to escape: these minima mark the centers of icicles in the escape time plot, as observed by Tiyapan and Jaffé and Mitchell. The central stable segment leaves a hole in the plot.

In the laboratory it is most natural to measure a photon's time to escape, but for

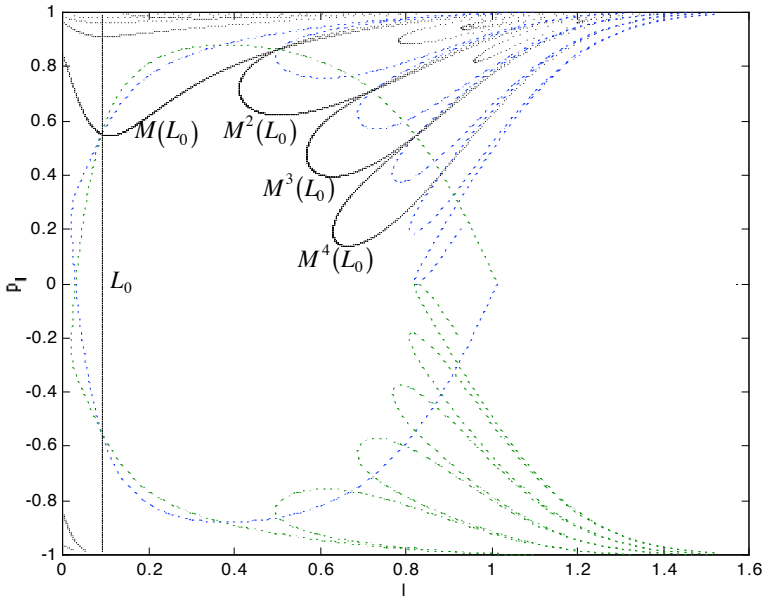

Figure 2.17: **Evolution of Line of Initial Conditions**

theoretical purposes one may instead compute the number of bounces to escape. In place of the time escape-time diagram consider a "discrete escape time" diagram (the plot of the number of bounces before a photon reaches the detector). Now the icicles appear as connected segments of l_0 escaping in a constant number of bounces (Figure 2.19). (Note that the escape time now appears on the y-axis, as the dependent variable; the region shown neighbors the stable region from below.)

Following Mitchell, we identify the prominent sequences of escape segments as epistrophes. Each epistrophe begins at an initial bounce number (iterate of M) and thereafter each includes one escape segment for each successive bounce. Our data confirm that epistrophes seem to be infinite sequences converging upon points on L_0. Escape segments grow smaller at higher iterates, and Mitchell has shown that the ratio of successive escape segment lengths asymptotically converges to the Liapunov exponent of the principal unstable fixed point.

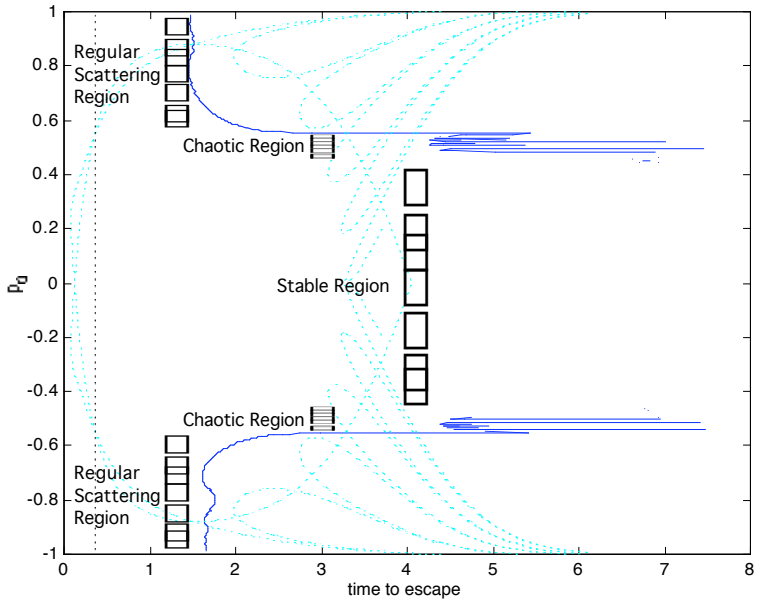

Figure 2.18: **Time To Escape** superimposed on surface of section

More epistrophes appear at higher iterates in the discrete time plot, featuring smaller initial (and subsequent) escape segments with the same properties as the main epistrophe. These new sequences converge on the endpoints of each escape segment in the first epistrophe; in general and for all time, two epistrophes appear and flank each escape segment delta iterates later. For this system $\Delta = 12$. We discuss this "epistrophe start rule" later.

This combination of rules imposes fractal order on the escape-time diagram: repeated structure within structure at all levels of resolution. Figure 2.20 compares sections of the escape time plot at successive levels of resolution in p_{l0}: the features at larger scales repeat at smaller scales. New features also appear at some levels of resolution, escape segments that are not connected to larger-scale structure. These new icicles spawn epistrophes of their own but are not members of any previous epistrophes. We mark one of these "strophes" with an asterisk.

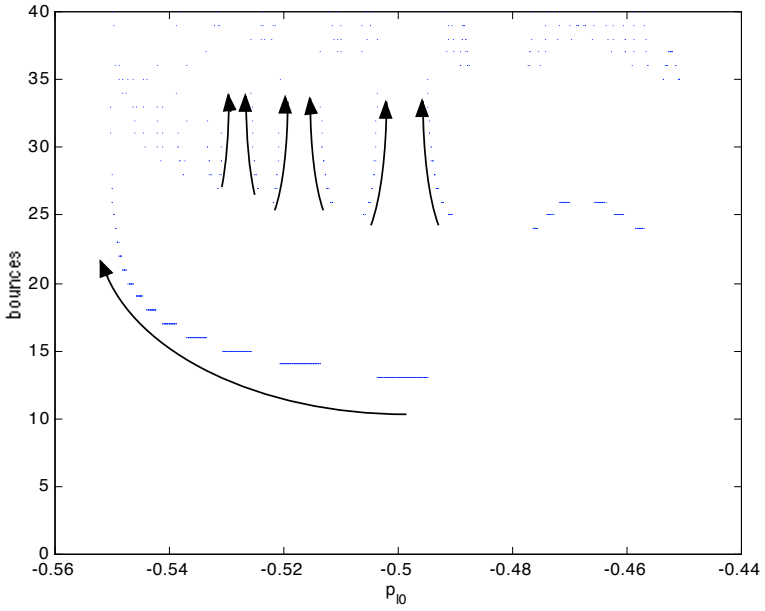

Figure 2.19: **Discrete Escape Time**

Such epistrophic fractals appear in many physical systems including ionization of hydrogen in parallel electric and magnetic fields. Open chaotic systems satisfying a few requirements may possess the necessary homoclinic tangle to force such fractal structure. Chapter 3 presents homotopic lobe dynamics to partially explain and predict this structure; we apply it to our system in Chapter 4.

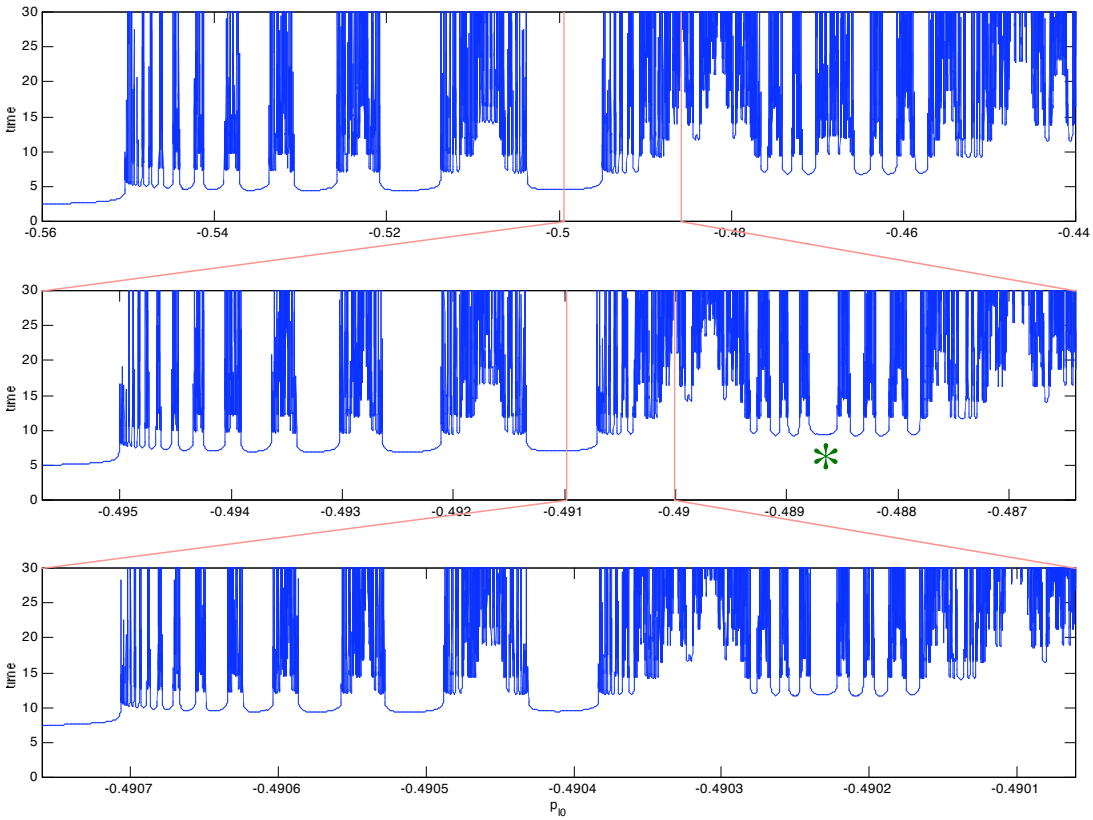

Figure 2.20: **Fractal Structure in Time To Escape**

Chapter 3

Homotopic Lobe Dynamics

We now provide the mathematics to explain the escape-time diagram by analysis of the surface of section. Homotopic lobe dynamics reduces the evolution of a curve in phase space to the evolution of an associated symbol sequence. Following Mitchell's method in [4] we use this model to prove the existence of a minimal required set of escape segments, describe a simple algorithm to generate this set, and show how recursion in this algorithm explains the spawning of new epistrophes near escape segments. The symbolic dynamics requires the introduction of new terminology for regions of the surface of section, whence we begin.

Consider a simple homoclinic tangle (Figure 3.1)[1]. The stable and unstable manifolds bound and define an invariant region of the phase plane, the *active region*: by continuity and orientation preservation, M maps all the points in the invariant region back into the region, and points outside the region (regular scattering trajectories) never enter it. The trajectories of interest all lie inside the active region. The middle

[1]Figures in this chapter are adapted from Mitchell [4].

of the active region, bounded on top by the stable manifold and below by the unstable manifold, is the *complex*. All bound trajectories stay in the complex, but many escape. A series of successive *capture zones* map into the complex from below the unstable manifold, and a mirror-image sequence of *escape zones* leave the complex above the stable manifold. Orbits only leave the complex through the escape zones, and only enter through the capture zones. Orbits that leave the complex may never return, hence we redefine escape as exiting the complex through escape zone E_0.

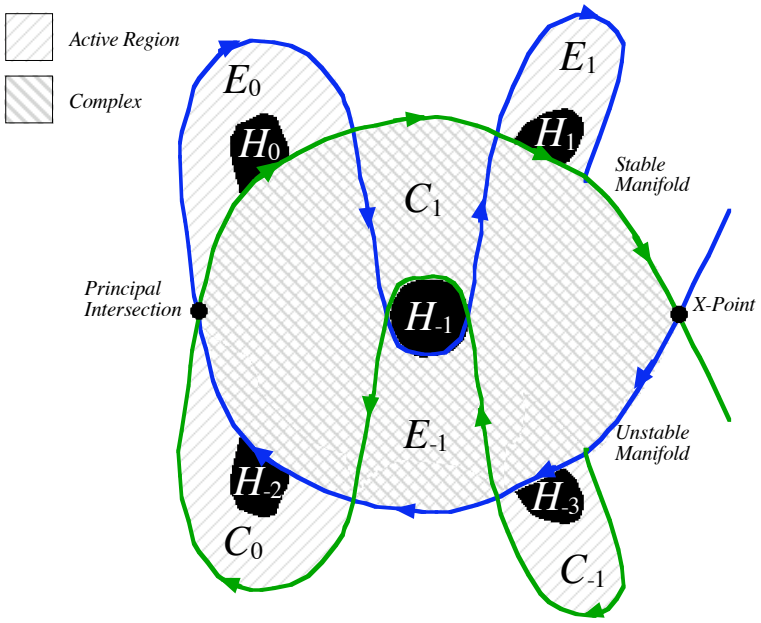

Figure 3.1: **Surface of Section**

The tangle inside the complex forces intersections of capture and escape zones which facilitate transport through the complex. All of the area that maps into the complex via zones C_{-1}, C_0, C_1 *etc.* sooner or later escapes through zones E_{-1}, E_0, E_1 *etc.* The escape zones and capture zones intersect an infinite number of times, and as there is an infinity of escape zones in the complex (pre-images of E_0), there is no upper bound on the number of iterates that a trajectory may spend between C_0 and E_0. There is however a lower bound—the minimum number of iterates a scattering trajectory

may spend in the complex depends on the first intersection $E_{-n} \cap C_n$, dependent on the topology of the complex. We call this the minimum delay time, D:

$$D = 2n - 1 \tag{3.1}$$

In Figure 3.1, capture zone C_1 intersects escape zone E_{-1} in a shaded region H. Thus $D = 1$: all pre-images $M^{-n}(H)$ lie in capture zones C_0, C_{-1}, ... outside the complex and all images $M(H)$ are in escape zones outside the complex. We call the special intersection H and all its images past and future *holes*: the set of all orbits that spend a minimal number of iterates in the complex.

The rules of the surface of section regulate the intersections of escape zones and capture zones. Continuity implies that any intersection between C_n and E_m forces an infinite family of related intersections, $...C_{n-1} \bigcap E_{m-1}, (C_n \bigcap E_m), C_{n+1} \bigcap E_{m+1}, ...$ which are all images or pre-images of $C_n \bigcap E_m$; by area preservation these intersections all have equal areas. The complex has finite area of course—capture zones must intersect escape zones and vice versa, so long as continuity is not violated and the stable and unstable manifolds do not cross themselves. These requirements cause fantastic undulations in the tangle (Figure 3.2). Asymptotic narrowing and stretching packs filament-like lobes infinitesimally close to the boundary of the active region.

Any line of inital conditions L_0 passing transversely through a finite region of the complex intersects the pre-images of E_0 an infinite number of times. This is the real cause of escape segments: intersections $L_0 \bigcap E_{-n}$ form segments at iterate n in the discrete escape time plot. We now present a method to predict the order and timing of a minimal set of these segments.

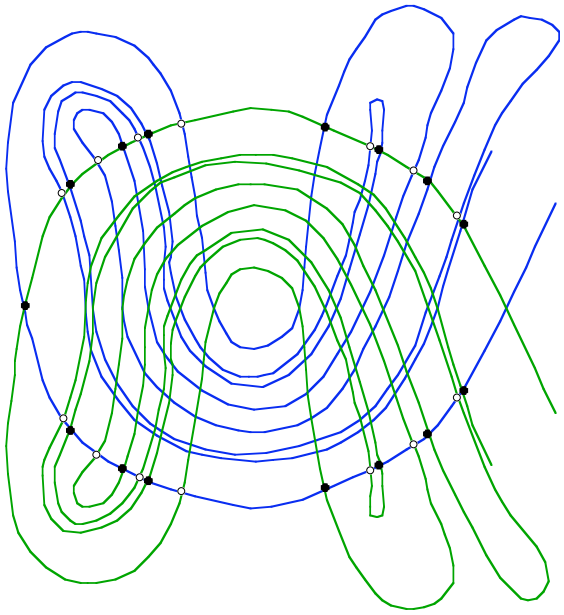

Figure 3.2: **Homoclinic Tangle**

3.0.3 Homotopy Classes

Consider two very simple directed curves L_0, L_0' in the surface of section (Figure 3.3). Both stretch between the same two homoclinic points s_1 and s_2; their main distinction is that they pass on opposite sides of the hole H_{-1}. One may associate L_0, L_0' with the segments of manifolds bounding zone C_1: L_0 loosely follows the stable manifold and L_0' follows the unstable manifold. In one iterate the segments will map forward between points s_3 and s_4: $M(L_0)$ remains near the stable manifold, but $M(L_0')$ follows the unstable manifold and continuity forces it to wrap around the next hole, H_0. In fact we may use the location of holes in the complex to determine the forced escape segments of arbitrary curves. We formalize this idea by defining homotopy classes of topologically similar curves with similarly ordered forced escape segments and by decomposing lines of initial conditions in terms of a basis of such classes.

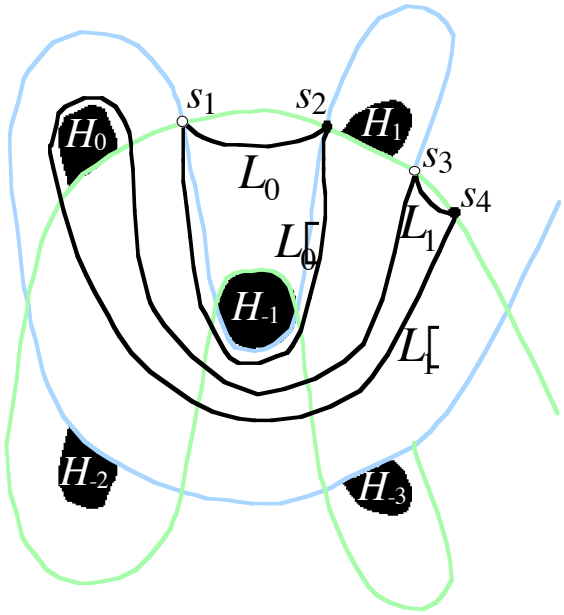

Figure 3.3: **Topological Forcing**

Two curves on the surface of section are said to be *homotopic* if they share the same endpoints and can be smoothly distorted into one another without crossing any holes or moving the endpoints. In Figure 3.4, curves A and B are homotopic; curve C passes on the other side of a hole and curve D has its own endpoints, so these are not homotopic to A and B.

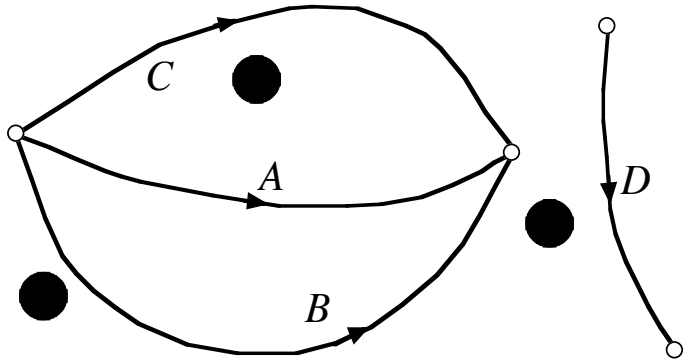

Figure 3.4: **Homotopic Curves**

A maximal set of homotopic curves defines a homotopy class of paths, or a *path class*. There are an infinite number of path classes in our surface of section corresponding to all possible endpoints and topologically distinct paths between holes. We are only concerned with paths beginning and ending on homoclinic points. Therefore, we label four sets of very simple directed curves on the surface of section:

1. S_n: sections of stable manifold bounding the active region clockwise
2. U_n: sections of unstable manifold bounding the active region clockwise
3. E_n: sections of stable manifold bounding the complex clockwise
4. C_n: sections of unstable manifold bounding the complex clockwise

We assume all of these curves connect adjacent homoclinic points; hence they are the shortest curves we consider. None of these curves may be smoothly distorted into one another without crossing holes or moving endpoints, so they each belong to a distinct well-defined path class, denoted respectively by s_n, u_n, e_n and c_n (Figure 3.5).

We may combine these simple paths by multiplication and inversion. Two paths classes a_1 and a_2 may be composed into a new path class a_1a_2 if the terminal point of a_1 is the origin point of a_2. Paths in a_1a_2 are homotopic to any two paths in a_1 and a_2 traversed sequentially. We define the inverse of a path class a, a^{-1}, as the set of all paths in a traversed backwards. The product of any path class with its inverse is the identity path class 1, the set of all paths beginning and ending at the same point without encircling any holes; a product class $a1$ or $1a$ reduces to a. These properties, save for the restriction that multiplication must be between adjacent paths, are the definition of a mathematical group. Hence we may say that s_n, u_n, e_n and c_n comprise

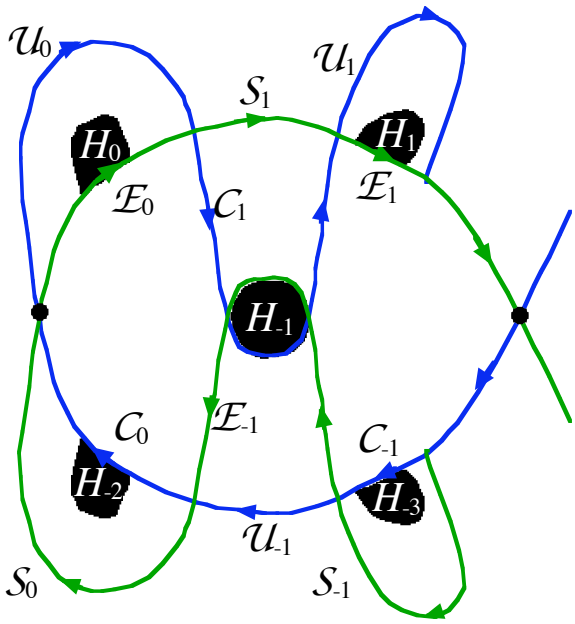

Figure 3.5: **Simple Paths in the Active Region**

a *groupoid* of paths between homoclinic points that do not intersect holes. The action of M on an entire path class is simply to shift its index:

1. $M(s_n) = M(s_{n+1})$
2. $M(u_n) = M(u_{n+1})$
3. $M(e_n) = M(e_{n+1})$
4. $M(c_n) = M(c_{n+1})$

3.0.4 The Basis of Path Classes

Within our groupoid are sufficient path classes to compose path classes between any two homoclinic points and around any number of holes in any order. Hence the

elements s_n, u_n, c_n, e_n form a spanning set for the groupoid of path classes. By eliminating redundant path classes we may define a minimal spanning set, or basis, of path classes such that all homoclinic points may be connected and a loop may be constructed around any hole. Most of the path classes are required, but holes within the complex may be surrounded by either $s_n c_n^{-1}$ or $u_{-n} e_{-n}^{-1}$ pairs; following Mitchell we choose the former and omit the latter from our basis. The basis is

1. $(..., s_{-1}, s_0, s_1, ...)$
2. $(..., u_{-1}, u_0, u_1, ...)$
3. $(..., c_{-1}, c_0, c_1, ..., c_D)$
4. $(e_0, e_1, ...)$

These path classes satisfy: (1) no paths in the basis intersect any paths except at endpoints; (2) each E_n and C_n encircles one hole and each hole is encircled once; (3) all homotopy classes in the groupoid have a unique finite reduced expansion in the basis. (Reduced expansions do not include any aa^{-1} pairs.) [4]

Let us decompose a line of initial conditions in this basis. The line L_0 belongs to a well-defined path class l_0, which by (3) above may be decomposed into a product of basis path classes. Decomposition is equivalent to stretching L_0 like a rubber band until it follows segments between adjacent homoclinic points all around the tangle (encircling holes in the complex with segments homotopic to C_n, S_n as opposed to U_{-n}, E_{-n}) (Figure 3.6).

M acts on the decomposed path class l_0 to advance the indices of each basis factor in turn, *e.g.*, $M(e_0 s_1) = e_1 s_2$ (recall $l_0 = e_0 s_1$). The forward iterates of l_0 will

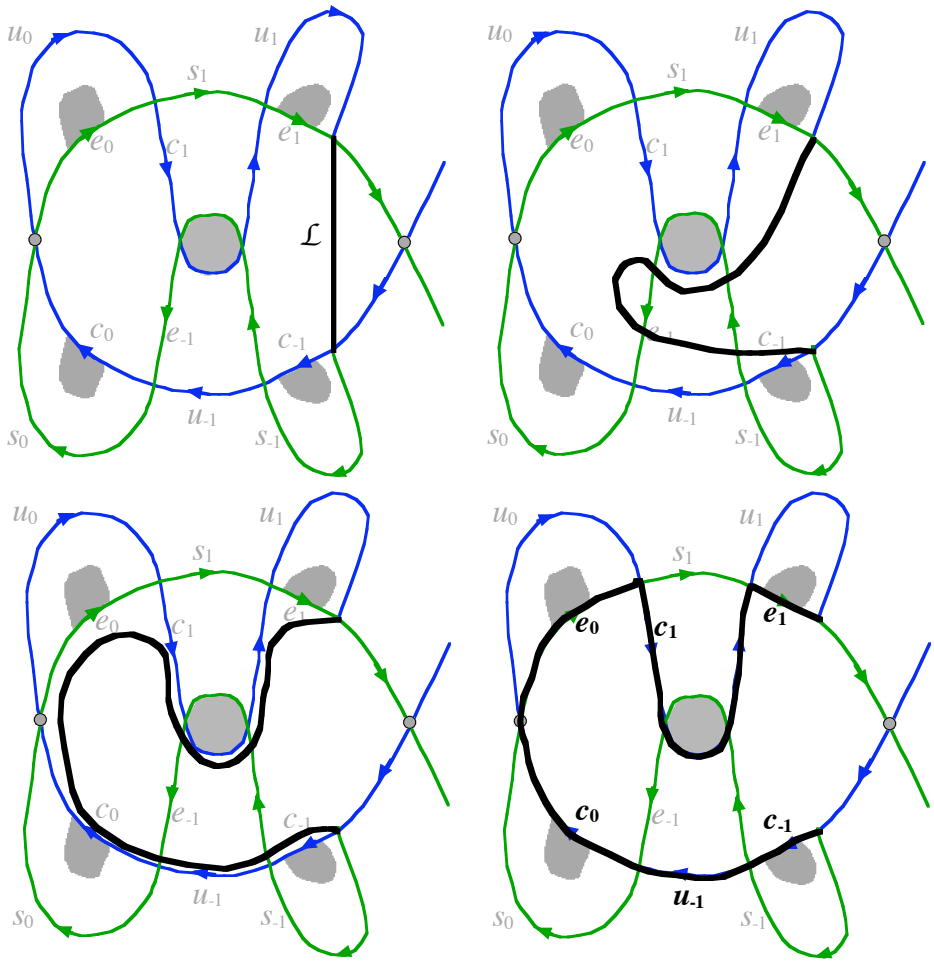

Figure 3.6: **Decomposition of a Curve**

automatically be expressed in the basis except for $M(c_D) = c_{D+1}$, which is excluded from the basis. This element must be itself decomposed by a lengthy unwinding process:

$$M(c_D) = F_{-1}u_0^{-1}e_0Fs_{D+1} \tag{3.2}$$

with

$$F = c_1 e_1 c_2 e_2 ... c_D e_D. \tag{3.3}$$

One may verify that this decomposition is correct by looking at a picture.

3.0.5 Symbolic Representation of Escape

A path L of path class l intersects the escape zone E_0 once for every occurrence of u_0 or u_0^{-1} in its decomposition. This is clear from a graph of the tangle: the segment U_0 bounds E_0 on the outside; any path homotopic to U_0 in the active region is forced to cross through E_0. Either u_0 or u_0^{-1} may be present in the decomposition, depending on the direction of L as it passes through E_0: if L travels clockwise around hole H_0 it will include u_0; if it travels counterclockwise it will include the inverse, u_0^{-1}. Thus many of the escape segments on a line of initial conditions L_0 may be identified by decomposing its path class l_0 and mapping it forward, watching for the u_0 segments. Mitchell justifies this algorithm in an appendix in his paper; we simply list key results here.

1. Iterate l_0 N times; each u_n or u_n^{-1} factor ($n \geqslant 0$) in the expansion of l_N corresponds to a segment that escapes in $N - n$ iterates.

2. The relative positions of the u_n-factors in the expansion of l_N are the same as the relative positions of their corresponding escape segments along L_0.

3.0.6 Implications

With an algorithm to predict forced escape segments on nearly arbitrary lines of initial conditions one may prove two rules about epistrophes in the discrete escape-time plot, which Mitchell derives and names the *Epistrophe Start Rule* and the *Epistrophe Continuation Rule*. His derivations are rigorous but both results may be understood more simply.

Epistrophe Continuation Rule: Every segment (in the minimal set) that escapes at $N-1$ iterates has on its side a segment that escapes at N iterates. This is the definition and origin of epistrophes in the escape-time plot. Consider a path class l that includes the factor c_D. When mapped forward, $M(c_D) = F^{-1}u_0^{-1}e_0Fs_{D+1}$ —the existence of a u_0 term implies an escape segment. In fact, $M(c_D)$ is the only way a u_0 can arise in the basis of path classes, because all u_n, $n < 0$ are excluded from the basis. Note as well that the definition $F = c_1e_1c_2e_2...c_De_D$ includes a c_D term. We reason: (1) the presence of an escape segment (a u_0 factor) implies a preimage factor c_D; (2) each $M(c_D)$ includes two new c_D factors which will include u_0 factors in one iteration; thus (3) the presence of an escape segment implies two more escape segments in the subsequent iterate.

Epistrophe Start Rule: Every segment that escapes at $N-\Delta$ iterates ($\Delta = D+1$) spawns immediately on both of its sides a segment that escapes at N iterates. We note that $M(F) = c_1^{-1}u_0^{-1}F$ and $M(F^{-1}) = F^{-1}u_0c_1$. Hence $M^{D-1}(F)$ includes a c_D^{-1}; $M^D(F)$ includes a u_0 and, from $M(c_D)$ above, we see $M^{D+1}(c_D)$ includes the pair u_0 and u_0^{-1}. These we identify as new epistrophes Δ iterates after the original escape segment.

The algorithm notably does not explain segments which are not forced by the holes. A full epistrophic fractal may include strophes at arbitrary iterates, which may or may not follow the Epistrophe Start Rule or Epistrophe Continuation Rule. It is generally believed that to predict all the escape segments would require an infinity of topological parameters; homotopic lobe dynamics today only considers the finite decomposition of a line of initial conditions and the minimum delay time of the tangle, so it is limited to description of the forced recursive structures.

3.0.7 Summary

Homotopic Lobe Dynamics identifies paths in the phase plane with path classes of like topology. Path classes may be decomposed in a specially selected basis of path classes. The action of M on these basis path classes is simply defined for all interesting classes except c_D, because c_{D+1} is excluded from the basis and must be decomposed into the basis. Escape segments may be identified with occurrences of u_n and u_n^{-1} factors in a path class decomposition. The algorithm for finding these segments becomes the basis for the Epistrophe Continuation Rule and the Epistrophe Start Rule which we see in the discrete escape-time plot. We can now apply this mathematics to the surface of section for the fish cavity.

Chapter 4

Results And Analysis

We now turn to the analysis of our system. We have demonstrated that the time-to-escape diagram has epistrophic fractal structure; we say the system obeys the Epistrophe Continuation Rule and the Epistrophe Start Rule, and its forced escape segments are predicted by Mitchell's algorithm. Separately, we predict the form of the pulse train that would be observed at the detector in the laboratory.

4.1 Confirming Epistrophic Structure

Recall that the minimum delay time D is determined by the first intersection $H_{-D} = C_n \cap E_{-n}$ in the surface of section, and this intersection maps forward and backward to generate the full set of holes H_n. In our system the first intersection is $C_6 \cap E_{-6}$, therefore $D = 2(6) - 1 = 11$ (Figure 4.1).

The Epistrophe Start Rule predicts that escape segments in epistrophes spawn flank-

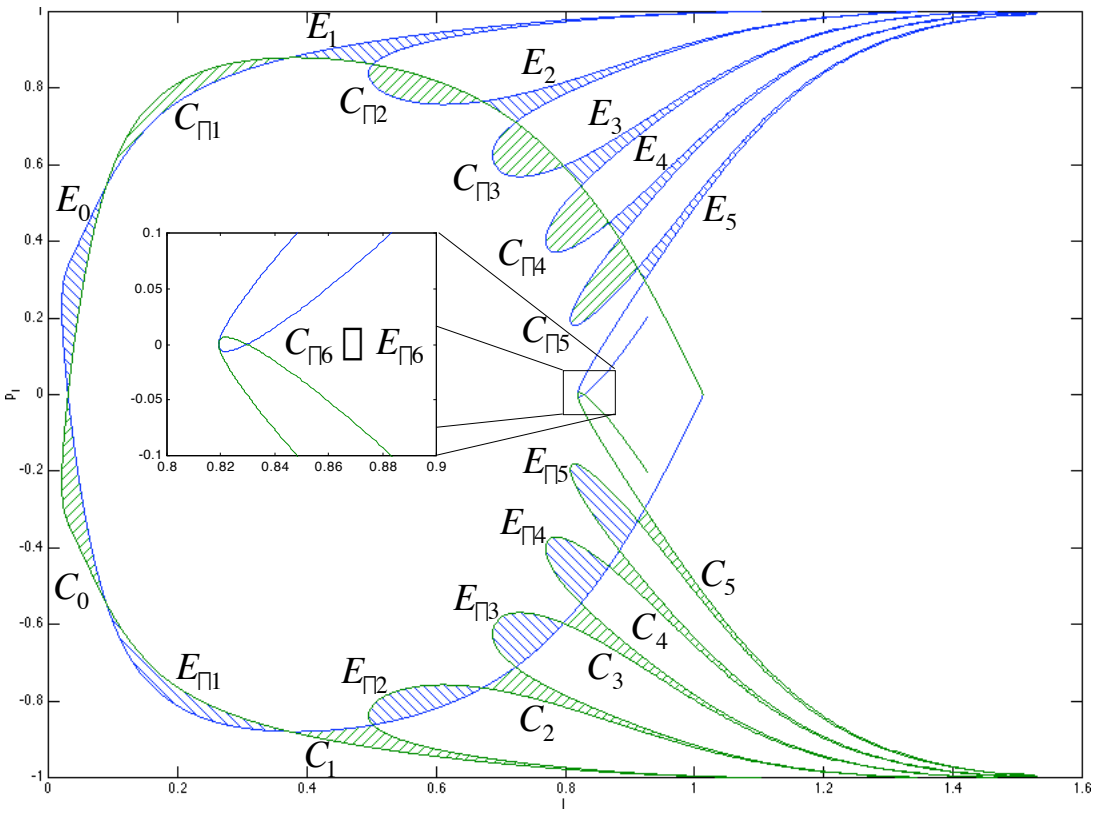

Figure 4.1: **Deriving** $D = 11$

ing epistrophes $\Delta = D + 1$ iterates later. This holds in our system for all iterates we simulate. Likewise, the Epistrophe Continuation Rule is responsible for the prominent converging series of escape segments between the stable region and the regular scattering regions of the line of initial conditions. Unsurprisingly, our plot has additional escape segments, some of them strophes, which are not part of these regular sequences. One may note that some of them spawn their own epistrophes as though following the rule; the current derivation of the Epistrophe Start Rule assumes that parent escape segments belong to epistrophes already, but the topology of the homoclinic tangle may tend to impose similar conditions on strophes. Relevant structures in our fractal are illustrated in (Figure 4.2).

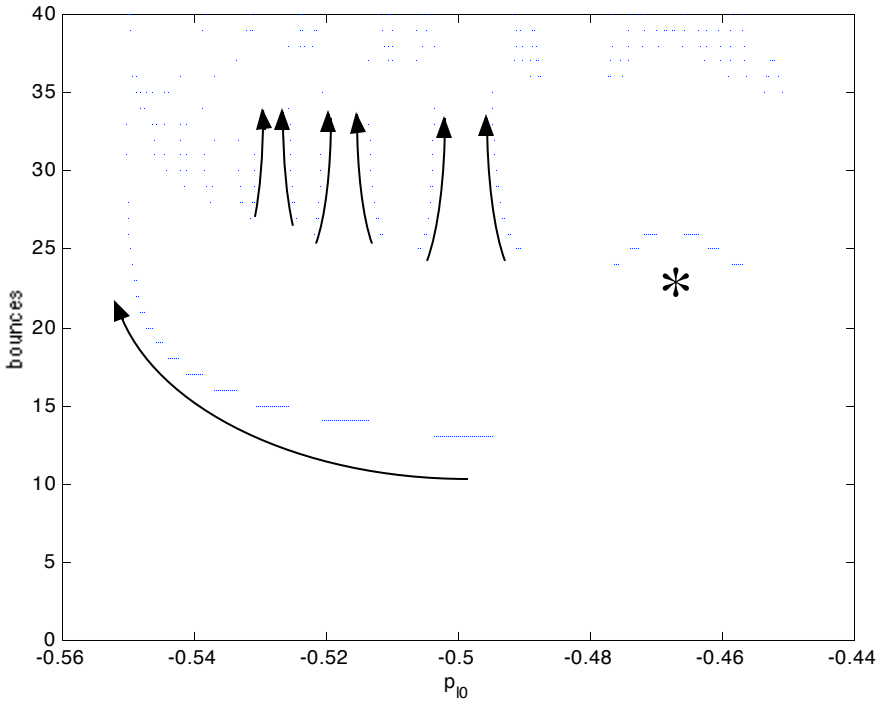

Figure 4.2: **Epistrophic Fractal Time To Escape**

We decompose our simple line of initial conditions into the product $l_0 = c_0 e_0$. It was desirable to choose the simplest possible initial conditions because under many iterations of M even a very simple curve may decompose into many terms. New sets of escape segments appear every $D+1$ iterates, so for $D = 11$ the decomposition of the initial conditions must map forward ten or twenty times before interesting features will appear. Hence we chose to place L_0 to the left of the stable zone (Figure 4.3).

By application of Mitchell's algorithm one may find $M(l_0)$, $M^2(l_0)$, etc[1].

$$l_0 = c_0 \tag{4.1}$$

[1]Following Mitchell, we omit terms e_n, $n \geqslant 0$ and all s_n from the symbol sequences because they do not result in escape segments or change the dynamics.

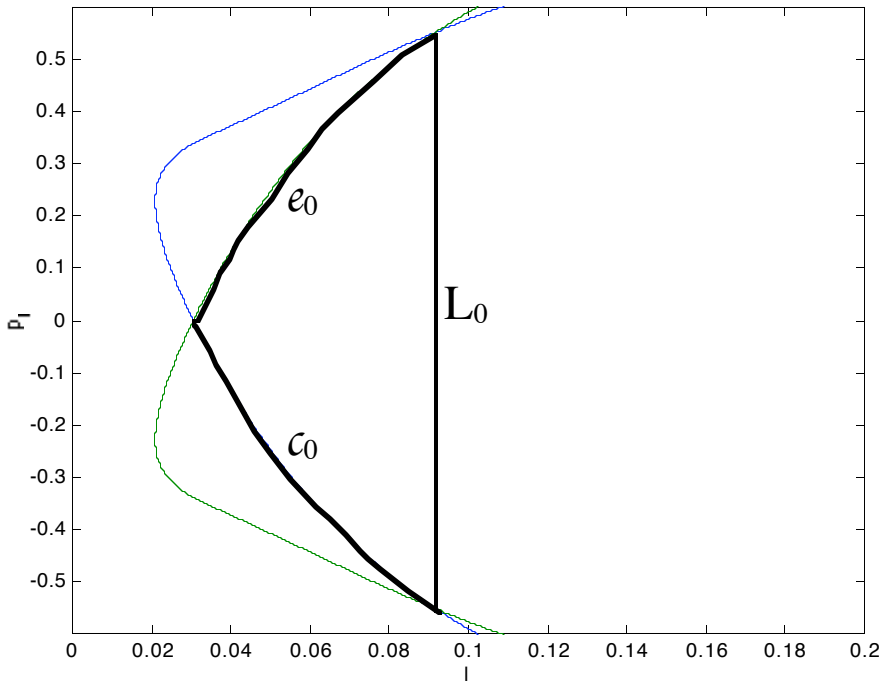

Figure 4.3: **Decomposition of Initial Conditions**

$$l_1 = c_1 \tag{4.2}$$

$$l_2 = c_2 \tag{4.3}$$

$$\cdots \tag{4.4}$$

$$l_{11} = c_{11} \tag{4.5}$$

$$l_{12} = F^{-1}u_0^{-1}F(\text{first escape segment}) \tag{4.6}$$

$$l_{13} = F^{-1}u_0^{-1}c_1u_1^{-1}c_1^{-1}u_0^{-1}F \tag{4.7}$$

This decomposition finally includes a u_0 at iterate 12, signifying one escape segment on that iterate. The next, l_{13}, has two u_0s and a u_1^-1, corresponding to the segment on iterate 12 and two on iterate 13. One may verify by hand that

$$l_{25} = u_0 u_1 \cdots u_{11} u_0^{-1} u_{12} u_0 u_1^{-1} u_0^{-1} u_{13}^{-1} u_0 u_1 u_0^{-1} u_{12}^{-1} u_0 u_{11}^{-1} u_{10}^{-1} \cdots u_0^{-1} \tag{4.8}$$

This correctly predicts the order escape segments up to and including 25 iterates (Figure 4.4). We focus on the two chaotic regions and omit the central stable region of p_{l0}.

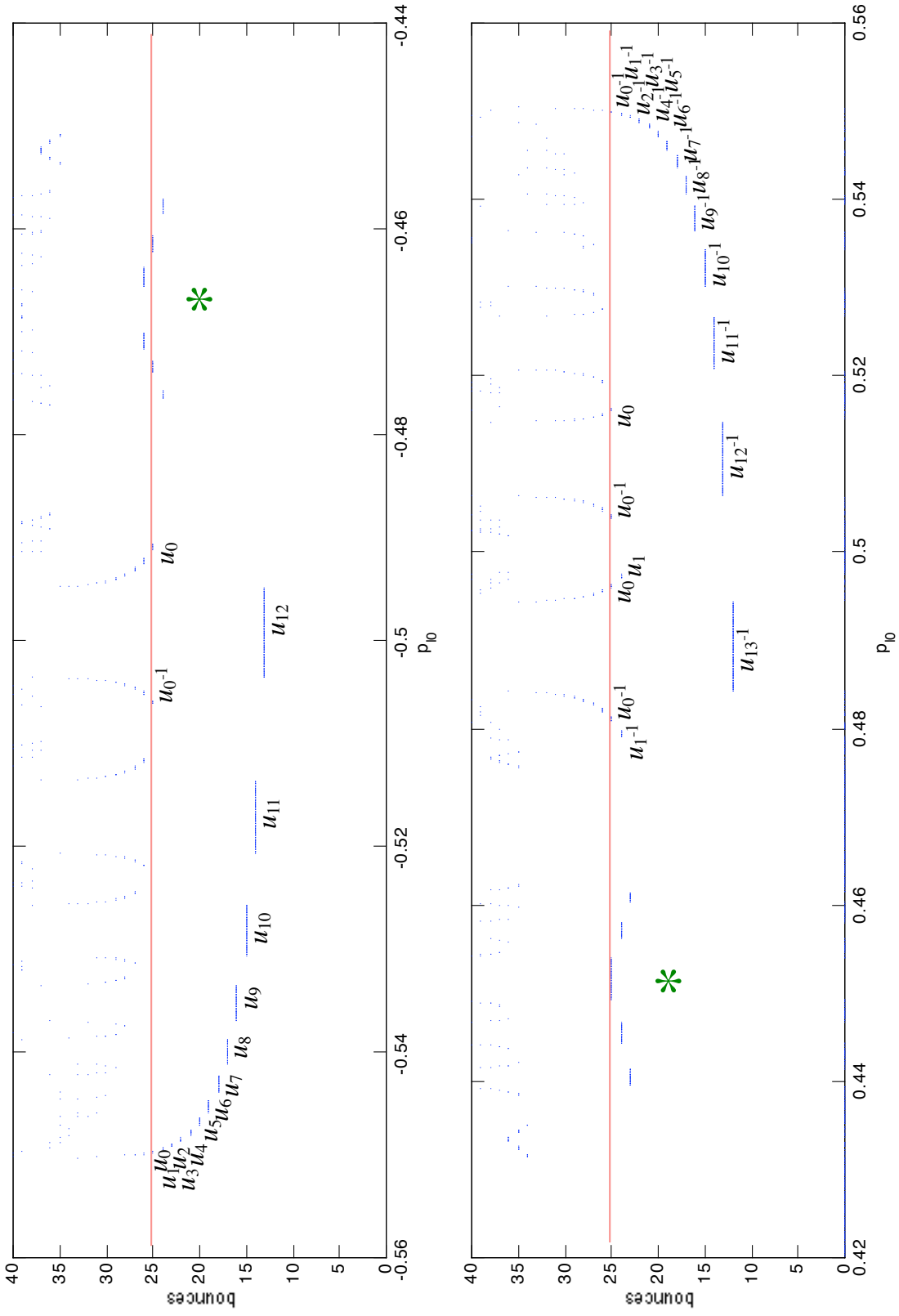

Figure 4.4: **Predicted Escape Segments for** $M^{25}(L_0)$

4.2 The Pulse Train

A histogram of time to escape over a set of trajectories gives a discretized representation of the pulse train seen at the detector. One burst of microwaves in a nonchaotic system would escape in a fairly simple time distribution, still recognizable as a pulse (though somewhat stretched out in time). Chaos—seen before in existence of discrete escape segments—maps a burst of initial conditions to a lengthy pulse train at the detector. Measurement of such a train should be possible in the laboratory and could provide a sense of the dynamics in the system[2].

Rather than use a histogram, we convolve the time to escape spectrum with a gaussian to obtain a continuous pulse train function. One may note the correlation between pulses and escape segments (Figure 4.5).

A uniformly distributed semicircular burst is not uniformly dense on the surface of section. Here we picked initial conditions following a density function $\rho = \arccos p_l$ corresponding to a point flash of microwaves in all directions.

[2]Whether the pulse train may be transformed to yield an escape-time plot is an area of active research.

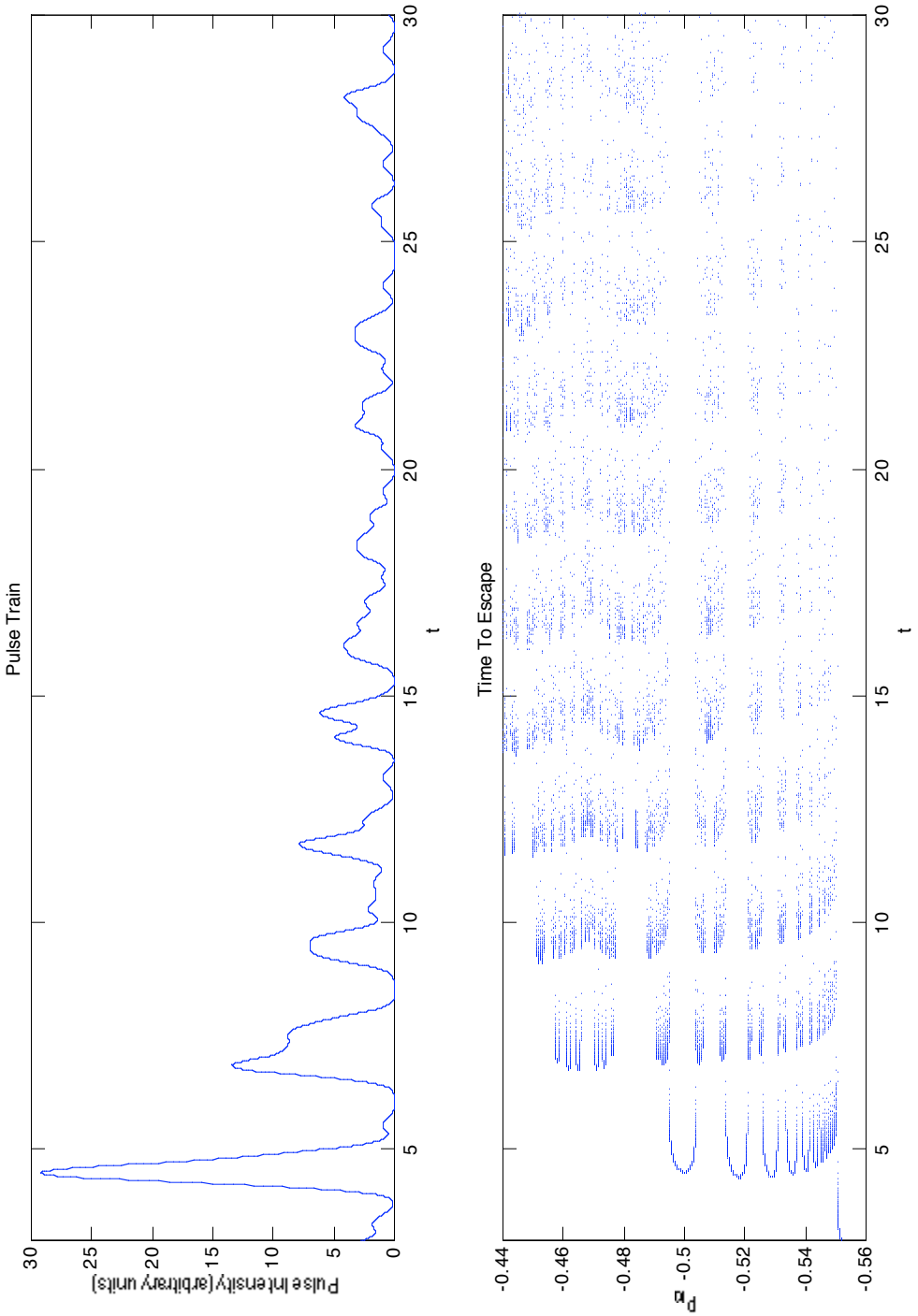

Figure 4.5: **Pulse Train**

Chapter 5

Conclusions And Future Work

The fish-cavity system was conceived as a lab-friendly analogue to the ionization of hydrogen in parallel electric and magnetic fields. We chose the shape of the reflecting cavity to satisfy the conditions for a Saddle-Center Map as described in [3], notably the presence of an unstable fixed point spawning a homoclinic tangle around a stable zone. Under classical dynamics the time a particle takes to escape such a system is highly sensitive to initial conditions; the plot of time to escape versus initial conditions has epistrophic fractal structure. We identify, analyze and explain this structure in our system, confirming that it is a suitable alternative to the hydrogen system. A single burst of photons in the cavity will lead to a chaotic pulse train exiting the system. We predict the shape of this pulse train for a particular line of initial conditions.

This simulation may be extended to predict steady-state interference patterns on a planar detector. Interference effects cannot be modeled by simply assigning a phase to trajectories. A correct model has to include Maslov indices, which requires analysis of the optical properties of the fish cavity. This extension would be a valuable addition

to the simulator.

Finally, this system remains to be tested. Being two-dimensional it is well-suited to tabletop microwave experiments and in fact bears resemblance to experiments being done now by Prof. Srinivas Sridhar of Northeastern University. Such an experiment would provide a valuable test of Homotopic Lobe Dynamics. We look forward to seeing our system tested fully in the laboratory.

Appendix: Implementation Notes

5.1 Trajectories

We represent trajectories parametrically by their current position $\overrightarrow{x}$ and velocity $\overrightarrow{v}$ (normalized to the speed $c = 1.0$ in simulation units). The simulator calculates the time Δt for a trajectory to intersect the wall of the cavity and advances the trajectories as

$$x_1 = x_0 + v_x \Delta t \tag{5.1}$$

$$v_1 = v_0 + v_y \Delta t \tag{5.2}$$

The cavity is represented by the "fish function"

$$y = f(x) = \pm\sqrt{x}\left(\frac{w}{2} + A(x - L)^2\right) \tag{5.3}$$

We substitute the parametric equations 5.1 into the fish function 5.3 to find the

intersection of the trajectory with the wall. The numerics are simplified by squaring the resulting equation, thereby obtaining the "intersection polynomial"

$$P(t) = (y - f)^2 = 0 \tag{5.4}$$

which conveniently eliminates the need to distinguish between intersections on the $y > 0$ and $y < 0$ sections of the cavity. Finding roots of polynomials numerically is fast and accurate; Matlab has functions to handle this for us. This fifth-degree polynomial in t has, in general, real and complex roots, which we classify as follows:

- Positive real roots: intersections in the future, $\Delta t > 0$
- Negative real roots: intersections in the past, $\Delta t < 0$
- Vanishing real roots: the trajectory's current position on the wall
- Complex roots: no physical intersection

The smallest positive real root $\Delta t = t_{min}$ corresponds to the first intersection of the trajectory with the fish curve in the future, by which we may calculate the new position. Sometimes the current position on the wall, the root $t = 0$, appears as an intersection in the future (albeit with very small $0 < t \ll 1$). We omit these roots by requiring t_{min} to surpass a threshold value $t_{small} = 10^{-12}$. In practice this allows extremely tangential trajectories (whispering gallery modes) to pass through the wall, but such trajectories are outside our region of interest and we do not create them.

Reflection conserves speed, so we reverse the trajectory's velocity normal to the curve, $v_\perp$:

$$\overrightarrow{v}_{next} = \overrightarrow{v}_{\parallel} - \overrightarrow{v}_{\perp} = 2(\overrightarrow{v} \cdot \hat{f}_{\parallel})\hat{v} - \overrightarrow{v} \tag{5.5}$$

where $\overrightarrow{f}_{\parallel}$, the tangent vector to the fish curve, may be calculated by either of two formulations:

$$\overrightarrow{f}_{\parallel} = \left(1, \frac{dy}{dx}\right) = \left(1, \frac{df}{dx}\right) \tag{5.6}$$

$$\overrightarrow{f}_{\parallel} = \left(\frac{dx}{dy}, 1\right) = \left(2y\left(\frac{d}{dx}f(x)^2\right)^{-1}, 1\right). \tag{5.7}$$

Analytically, the methods lead to the same $\hat{f}_{\parallel}$, but the numerical error is different. In the regime $x \ll 1$,

$$\Delta\frac{dy}{dx} \propto x^{-1/2} \tag{5.8}$$

$$\Delta\frac{dx}{dy} \propto 1. \tag{5.9}$$

At points where the curve flattens so $\frac{df}{dx} \simeq 0$, there is a singularity in $\frac{dx}{dy}$. We chose the most accurate method for different sections of the curve by considering a plot of $1 - \frac{dy}{dx}\frac{dx}{dy}$ (Figure 5.1) and estimating the point at which error was minimized. For small x, most of the error comes from $\frac{dy}{dx}$, but for larger x the error is due to $\frac{dx}{dy}$. In practice we use $x_{cutoff} = x_{stable}/3$ as it remains a good approximation for various L (bottleneck positions).

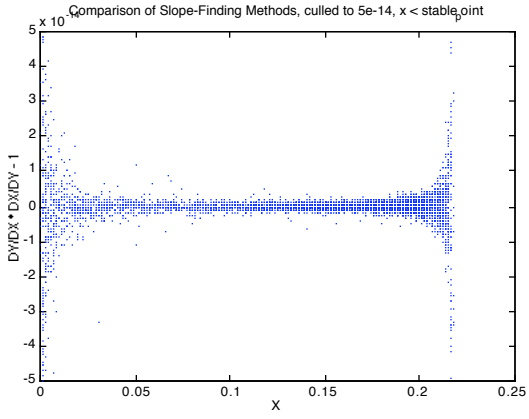

Figure 5.1: **Choosing Cutoff Point**

5.2 Surface Of Section

Arc-length momentum p_l in the surface of section is identical to $v_\parallel$ as calculated above, and we use the same precautions to maximize accuracy. The arc-length coordinate l is the path length along the curve wall, found by either of two integrals:

$$l(x) = \int_{x=0}^{x_{orbit}} \sqrt{1 + \left(\frac{dy}{dx}\right)^2}\, dx \tag{5.10}$$

$$l(y) = \int_{y=0}^{y_{orbit}} \sqrt{1 + \left(\frac{dx}{dy}\right)^2}\, dy. \tag{5.11}$$

Neither of these can be evaluated analytically, so we integrate them numerically using Matlab's ODE solvers. For $x < x_{cutoff}$, we use $l(y)$. Unfortunately, simply integrating $l(x)$ as in equation 5.10 still relies on $\frac{dy}{dx}$ near the origin and is prone to error. Thus we split the calculation into two parts:

$$l(x) = \int_{y=0}^{y(x_{cutoff})} \sqrt{1 + \left(\frac{dx}{dy}\right)^2}\, dy + \int_{x_{cutoff}}^{x_{orbit}} \sqrt{1 + \left(\frac{dy}{dx}\right)^2}\, dx \qquad (5.12)$$

It is impractical to calculate l numerically for every bounce of every trajectory. Thus we pre-calculate two tables, $l(x)$ and $l(y)$, each with about 150 elements. The mapping $\overrightarrow{x} \rightarrow l$ is implemented by a table lookup in either $l(x)$ or $l(y)$. Cubic spline interpolation (built in to Matlab) creates the best l value based on the lookup. Error is minimal locally; globally it can never be worse than the error of the nearest table entries. This is sufficient for our purposes—the surface of section is merely output and does not affect the simulator map M.

5.2.1 Tracing The Manifolds

Plotting the unstable manifold requires placing a line of initial conditions as near as possible to the manifold and mapping them forward. The unstable manifold has attractor-like properties which reduce error over time, so the principal difficulty is setting down a line of initial conditions which will match up head to toe from iterate to iterate (so that l_0, $M(l_0)$, $M^2(l_0)$ *etc.* are a set of uniformly distributed points on the manifold with no overlaps). We achieve this by starting a single pilot trajectory very near the unstable fixed point, $(l_0, p_{l0}) = (l_{unstable}, -\epsilon)$ with $\epsilon \ll 1$. This trajectory is mapped forward 40 times, such that its last two iterates (l_{39}, p_{l39}) and (l_{40}, p_{l40}) are both infinitesimally close to the manifold and still near the X-point. We generate an entire segment of initial conditions by interpolating between these points, which will map end-to-end along the unstable manifold.

Earlier we state without proof that the stable manifold is a reflection of the unstable

manifold. The stable manifold is the set of all trajectories that map forward asymptotically to the X-point. In reverse time, the stable manifold looks like the unstable manifold—the set of trajectories diverging from the X-point—except that momentum vectors still point "forward." We can therefore plot the stable manifold by reversing momenta of trajectories diverging from the X-point. On the surface of section, this is the reflection ($p_l \rightarrow -p_l$) of the unstable manifold.

5.2.2 Intersections With E_0

For a trajectory in the complex, we define escape as entering the escape zone E_0. We pre-plotted the unstable manifold (hence the stable manifold) to very high resolution and saved the sections bounding E_0. For efficiency we detecting escapes with a two-step process:

1. Bounding Box Check: does the trajectory fall into the rectangular bounding box around E_0? This step rapidly removes most trajectories from consideration.

2. Manifold Check: does the trajectory pass to the right of the unstable manifold and to the left of the stable manifold? This step uses cubic spline interpolation for maximum accuracy and is considerably slower than the bounding box check.

In a typical simulation of 10,000 trajectories, there are usually only one or two incidents when the simulator catches the same trajectory in the escape zone twice. The occasional error is most likely due to the resolution on the manifold segments and does not affect our analysis of the time to escape.

Bibliography

[1] Melissa Commisso, REU project report, College of William and Mary, 2003. (unpublished)

[2] Joel Handley, REU project report, College of William and Mary, 2001. (unpublished)

[3] K.A. Mitchell, J.P. Handley, J.B. Delos, S.K. Knudson, Chaos **13**, 880 (2003).

[4] K.A. Mitchell, J.P. Handley, J.B. Delos, S.K. Knudson, Chaos **13**, 892 (2003).

[5] K.A. Mitchell, J.P. Handley, B. Tighe, A.A. Flower, J.B. Delos, Phys. Rev. Lett. **92**, 073001 (2004)

[6] A. Tiyapan, Charles Jaffé, J. Chem. Phys. **99**, 2765 (1993).